

Modeling of time and frequency dependent behavior of viscoelastic multi-layered reinforced composites with imperfect interfaces

Ahmed Bouchikhi¹, Abderrahmane Bakkali^{1*} , Younes Abouelhanoune² 

¹ Faculty of Sciences, Abdelmalek Essaadi University, Tetouan, Morocco

² National School of Applied Sciences, Abdelmalek Essaadi University, Tetouan, Morocco

* Corresponding author's e-mail: a.bakkali@uae.ac.ma

ABSTRACT

In this work, a two-step homogenization strategy is developed to predict the frequency and time-dependent effective behavior of multi-layered reinforced viscoelastic composites with imperfect interfaces. In the first step, the modeling is based on the extension of a matrix formulation, initially developed for multi-layered elastic composites with perfect interfaces, to the case of multi-layered viscoelastic composites with imperfect interfaces. This extension is made by using the Laplace Carson transform to transform the linear viscoelastic constitutive law to another one analogous to the elastic one and an adapted linear spring model for viscoelastic imperfect interfaces. In the second step, the well-known Mori-Tanaka micromechanical model is used to estimate the effective behavior of each reinforced layer. The estimated effective behavior is injected into the developed matrix formulation to obtain the effective behavior of the considered multi-layered composite. The effective behavior is estimated both in the frequency and time domains. For comparison, a perfect hybrid model in which the interface is considered as an interlayer with an equivalent thickness is considered. Numerical results are presented in the frequency and time domains with respect to constituent volume fractions and imperfect interface effects. The developed approach allows one to design multi-layered viscoelastic composites taking into account the geometric and mechanical parameters of constituents.

Keywords: viscoelastic composites, multi-layered composites, Mori-Tanaka, imperfect interface, Carson-Laplace transform.

INTRODUCTION

Multi-layered composites are frequently used in many industrial fields, such as in automotive and aeronautics, aerospace and, naval. In order to design multi-layered composites with damping behavior for control and reducing noise, one has to introduce viscoelastic layers into the multi-layered composites. Viscoelastic composites have time dependent properties mainly at high temperature. Due to the importance of designing composite with light weight and improved damping properties many researchers have taken the challenge and developed models for predicting effective viscoelastic properties of composites in frequency and time domain. The issue of imperfect interfaces is crucial in designing multi-layered

composites and taking into account their effects in the modeling has taken the interest of many researchers. The physical phenomena behind the imperfect interfaces are sliding, debonding due non perfect adhesion, cracks, among others.

In the literature, one can find mainly two categories. The one based on the Laplace transform approach and the one developed directly in the time domain.

For the Laplace transform approach, Hashin [1-3], based on the correspondence principle and Laplace transform, derived explicit effective expressions for particulate and fibrous composites. Christensen [4] developed upper and lower bounds for viscoelastic composites. The previously mentioned literatures are based on the work of Hashin [5]. Brinson and Lin [6] used

micromechanics approaches to estimate the effective viscoelastic properties. Haberman et al. [7-9] extended the work of Cherkaoui et al. [10] to analyze and estimate the effective behavior of viscoelastic composites. Koutsawa et al. [11] used the work of Lipinski et al. [12] and extended it to the case of viscoelastic composites. Li and Sun [13] extended the work of Eshelby to the case of viscoelastic nano-composites with imperfect interfaces. Some researchers extended Laplace's approach combined with micromechanics to the case of visco-piezoelectric and visco-magneto-electroelastic, including [14-18].

For the second approach, which aims to derive the effective behavior directly in the time domain, one can find the one based on internal variables. This allows one to consider complex path loadings and ageing behavior. One can find the work of Lahellec and Suquet [19-20] investigating the effective linear viscoelastic behavior and the nonlinear viscoelastic and visco-plastic behavior of composites. Ricaud and Masson [21] extended the internal variable approach to ageing viscoelastic composites. Masson et al. [22] adapted the work developed in [21] to estimate the effective ageing viscoelastic behavior of polycrystal materials. Berbenni et al. [23] developed a new time-incremental internal variables approach based on the exact solution of the Eshelby inclusion problem. Other researchers developed modeling straightforward in the time domain based on a different approach. Sanahuja [24] developed a displacement based modeling combined with the Mori-Tanaka model to predict the effective time-dependent ageing behavior for viscoelastic composites with spherical inclusions. El kouri et al. [25-26] developed a straightforward time-dependent modeling based on the Eshelby inclusion problem for heterogeneous and multi-coated viscoelastic composites. Recently, Bakkali and El kouri [27] extended the formulation to the case of visco-piezoelectric composites. Barthélémy [28] extended the Eshelby inclusion problem to the case of ageing viscoelastic composites. Chen et al. [29] developed a finite strain model for particulate viscoelastic composites. Chen et al. [30] developed a modeling based on the correspondence principle, the strain energy contribution of each constituent combined with micromechanics principles, leading to a time-dependent closed-form expression for viscoelastic composites with spherical inclusion. This later work, extended by Chen et al. [31]

to the case of spherical multi-coated inclusions. Galadima et al. [32] developed a computation scheme based on a non-local homogenization method to estimate the effective behavior of viscoelastic composites. Recently, to tackle the issue of imperfect interfaces on effective behavior, Dinzart [33] investigated the imperfect interface effect, based on an equivalent inclusion replacement methodology, on the macroscopic effective viscoelastic behavior of viscoelastic composites with multi-coated inclusions. Another class of models in time domain is the one developed by Molinari et al. [34-35] to study the effective viscoelastic and viscoplastic behavior of composite materials. This approach is based on an affine linearization of the local and macroscopic behavior. Similarly, a sequential linearization method is developed by Kowalczyk and Petryk [36] to study and estimate the viscoelastic behavior of viscoelastic composites.

All the above-mentioned literature deals with reinforced viscoelastic composites. This paper is a contribution to modeling the frequency and time-dependent behavior of multi-layered reinforced composites. For modeling the effective behavior of multi-layered composites, one can find the work published by Kim [37] and Bouchikhi et al. [38] for multi-layered elastic composites. This later is extended by Kim [39] and Kim et al. [40] to the case of multi-layered multi-functional magneto-electroelastic composites. The matrix formulation, first developed in [37], was also used and derived in other published works [41-43] to study and estimate the nonlinear macroscopic behavior of laminated composites when martensitic transformations are induced in [41], and of bicrystals and duplex stainless steels in [42-43] respectively. Oscar et al [44] based on an asymptotic approach, investigated the modeling of imperfect viscoelastic interfaces in the case of multi-layered composites. In this paper a contribution is made by developing a two-step modeling procedure to estimate the effective behavior of multi-layered reinforced viscoelastic composites with imperfect interfaces. The novelty of this work is to extend the matrix formulation in [37] to the case of multi-layered viscoelastic composites with imperfect interfaces by the use of the Laplace Carson transform in the viscoelastic problem, transforming it to an analogous elastic one in the frequency domain, and by adapting the linear spring model to the case of imperfect

viscoelastic interfaces and then considering the Mori-Tanaka model to estimate the effective moduli of each reinforced layer and injecting it into the developed matrix formulation.

That way, the developed approach, called the imperfect hybrid model, contains two major steps: The first step is the development of the matrix formulation allowing one the estimation of the effective behavior of the multi-layered viscoelastic composite, including the imperfect interface effect. The second one is the estimation of the effective properties of each reinforced layer based on the Mori-Tanaka micromechanical model. The effective properties are first estimated in the frequency domain and then inverted numerically to the time one. The developed approach allows one to estimate the effective viscoelastic behavior of multi-layered reinforced composites in time and frequency domains while taking into account constituents' properties, the shape of reinforcement, the volume fraction of constituents, and the imperfect interface effect. In addition, a perfect hybrid model is considered when the imperfect interface is introduced as an interlayer with an equivalent thickness. It is remarked that the two considered models have the same estimation. Different numerical results are presented in frequency and time domains.

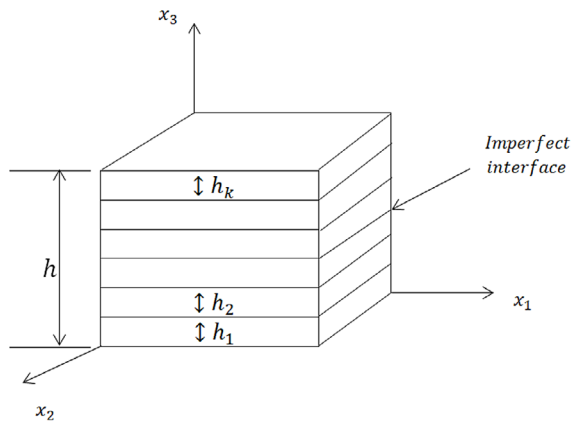


Figure 1. RVE of N-layer viscoelastic composite

MULTI-LAYERED CONSIDERED COMPOSITE AND BASIC EQUATIONS

The considered multi-layered composite and homogenization procedure

In this work, a viscoelastic multi-layered reinforced composite is considered. The representative volume element (RVE) of the composite is shown in Figure 1. It is constituted of N viscoelastic layers where each layer is reinforced with aligned short fibers. Layers are in the x_1 - x_2 plane and perpendicular to the x_3 axis. The interface between layers is considered imperfect. Fibers are considered aligned in the x_2 direction. The thickness, volume fraction, and viscoelastic relaxation tensor of the i^{th} layer are noted, respectively h_i , f_i , and $C_i(t)$. The volume fraction is obtained by $f_i = h_i / \sum_{k=1}^N h_k$ where $h = \sum_{k=1}^N h_k$ is the thickness of the RVE. The homogenization procedure followed in this paper to obtain the effective viscoelastic properties of the multi-layered composite is divided into two steps:

- Step 1: Consist of using the Mori-Tanaka mean field micromechanics model to derive the effective properties of each reinforced layer as illustrated in Figure 2.
- Step 2: Consist of using a matrix formulation allowing the derivation of the expression of the effective properties of the multi-layered composite where each reinforced layer is replaced by the homogenized one using the Mori-Tanaka model.

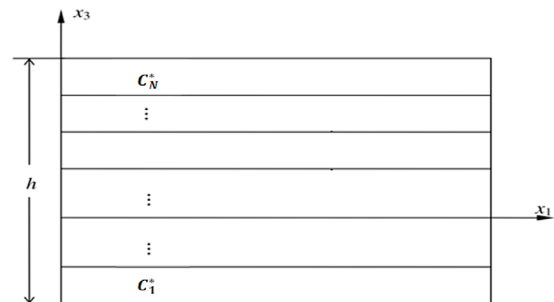


Figure 3. The multi-layered composite where each layer is replaced by the homogenized one

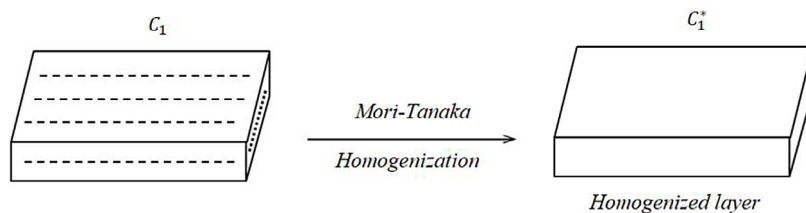


Figure 2. The homogenization of each reinforced layer of the viscoelastic multi-layered composite using the Mori-Tanaka model

Constitutive equations

The multi-layered composite is constituted of N -viscoelastic reinforced layers. All the constituents are considered viscoelastic, and their behavior is described by the linear viscoelastic correspondence principle. A representative volume element (Fig. 1) of volume Ω , is considered, and it is subjected at its boundary to the macroscopic strain $E(t)$ and displacement $u(x, t) = E(t) \cdot x$.

The constitutive equation modeling the linear non ageing viscoelastic behavior is given by:

$$\sigma_{ij}(x, t) = \int_0^t C_{ijkl}(x, t - \tau) \frac{\partial \varepsilon_{kl}(x, \tau)}{\partial \tau} d\tau \quad \forall x \in \Omega \tag{2.1}$$

where $C_{ijkl}(x, t - \tau)$ are the components of the relaxation tensor that give the viscoelastic response through the i, j directions at the time t when a unit strain is applied through directions k, l at the time τ .

In the Stieltjes space, Equation (2.1) is rewritten in a condensed form through a convolution product as:

$$\sigma_{ij}(x, t) = [C_{ijkl}(x) * d\varepsilon_{kl}(x)](t) \quad \forall x \in \Omega \forall t > 0 \tag{2.2}$$

The mathematical formulation in this work is established first in the frequency domain and then inverted to the time one. For this sake, the Laplace-Carson transform is used. The Laplace-Carson transform of a time-dependent function is given by

$$LC\{f\}(s) = \bar{f}(s) = s \int_0^{+\infty} e^{-st} f(t) dt \tag{2.3}$$

where s is the Carson variable and it is taken as $s = i\omega$ (the harmonic case is considered).

Applying the Laplace-Carson transform to the viscoelastic constitutive equation (Eq. (2.1)) leads to

$$\bar{\sigma}_{ij}(s, x) = \bar{C}_{ijkl}(s, x) \bar{\varepsilon}_{kl}(s, x) \tag{2.4}$$

where
$$\bar{C}_{ijkl}(s, x) = s \int_0^t e^{-su} C_{ijkl}(u, x) du$$

One can see that the application of the Carson transform reduces the viscoelastic problem to another one analogous to the elastic problem but expressed in the frequency domain. The relaxation tensor $\bar{C}_{ijkl}(s, x)$ has the same role as the elastic tensor in linear elasticity. To complete the governing equations in the frequency domain, the compatibility and the equilibrium equations, after applying the Laplace-Carson transform, are given by:

$$\bar{\varepsilon}_{ij}(x, s) = \frac{1}{2} (\bar{u}_{i,j}(x, s) + \bar{u}_{j,i}(x, s)), \quad \forall x \in \Omega \tag{2.5}$$

$$\bar{\sigma}_{ij,i}(s) = 0, \quad \forall x \in \Omega \tag{2.6}$$

Then the equilibrium equation, as in the time domain, is obtained in the frequency domain by:

$$(\bar{C}_{ijkl}(x, s) \bar{u}_{k,l}(x, s))_{,j} = 0 \quad \forall x \in \Omega \tag{2.7}$$

In this work, the considered multi-layered viscoelastic composites have imperfect interfaces between layers. The imperfect interfaces are denoted ' S ' (see Fig. 4) and the superscripts + and - indicate the positive and negative parts of the surface. As illustrated in Figure 4, one can see that the imperfect interface between the two layers (Fig. 4(a)) could be replaced by an interphase separating the two layers of thickness t (Fig. 4(b)). This equivalency is used in the numerical section for comparison and validation. In the following, the linear spring model is considered to describe imperfect interfaces.

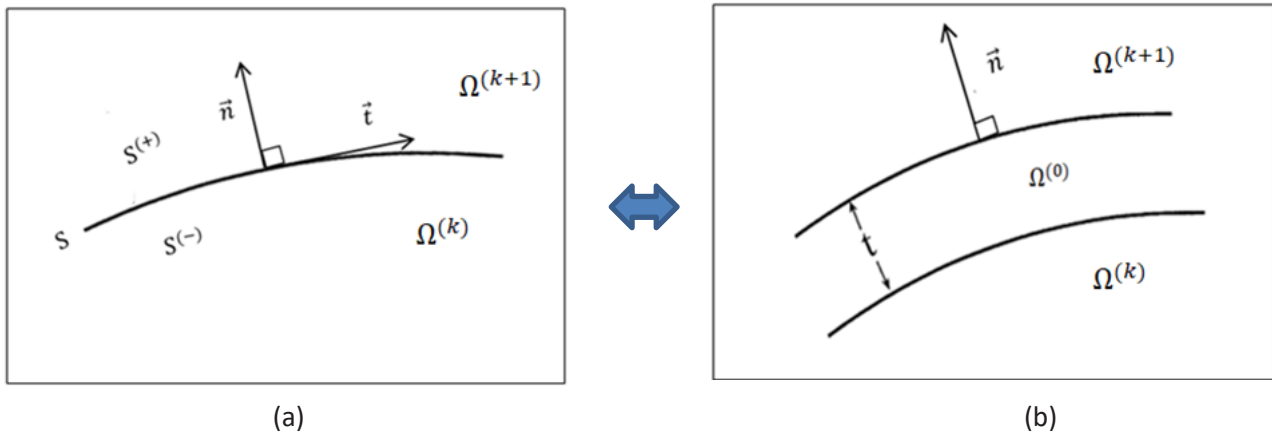


Figure 4. Imperfect interface effect: (a) the geometry of the imperfect interface, (b) the geometry of a thin interphase between two layers

Viscoelastic imperfect interface

To describe the mechanical behavior of viscoelastic imperfect interfaces, the linear spring model for elastic imperfect interfaces is extended here to the case of viscoelastic imperfect interfaces [13]. The linear spring model considers the discontinuity of the displacement jump and the continuity of traction over the interface. In the case of viscoelastic imperfect interfaces [13], the continuity of the time-dependent traction vector field across the interface 'S' is given by:

$$\left[\sigma_{ij}(t) \right] n_j = \left[\sigma_{ij}^{(k+1)}(t) - \sigma_{ij}^{(k)}(t) \right] n_j = 0 \quad (2.8)$$

where $\sigma_{ij}^{(k)}(t)$ stands for the time-dependent Cauchy stress tensor field over $\Omega^{(k)}$.

The interfacial displacement jump is time dependent, and it is expressed through an integral form relating the time-dependent displacement jump and traction vector through the viscoelastic compliance describing the time-dependent behavior of the imperfect interface [13]:

$$\left[u_i(t) \right] = \Delta u_i(t) = \int_0^t \psi_{ij}(t-\tau) \frac{\partial \sigma_{jk}(\tau)}{\partial \tau} d\tau n_k \quad (2.9)$$

with $\psi_{ij}(t)$ is the viscoelastic compliance of the imperfect interface given by

$$\psi_{ij}(t) = \alpha(t) \delta_{ij} + (\beta(t) - \alpha(t)) n_i n_j \quad (2.10)$$

$\alpha(t)$ and $\beta(t)$ are the interface compliance parameters related to the sliding and debonding effect.

Equation (2.9) is written in a condensed form through the following convolution product:

$$\left[u_i(t) \right] = \Delta u_i(t) = \left[\psi_{ij} * d\sigma_{jk} \right] (t) n_k \quad (2.11)$$

Applying again the Laplace-Carson transform on Equation (2.11) gives

$$\Delta \bar{u}_i(s) = \bar{\psi}_{ij}(s) \bar{\sigma}_{jk}(s) n_k \quad (2.12)$$

where $\bar{\psi}_{ij}(s) = s \int_0^t \psi_{ij}(v) e^{-sv} dv$ represents the Laplace-Carson transform of the compliance function.

The frequency dependent compliance is given by

$$\bar{\psi}_{ij}(s) = \bar{\alpha}(s) \delta_{ij} + (\bar{\beta}(s) - \bar{\alpha}(s)) n_i n_j \quad (2.13)$$

Applying the Laplace-Carson transformation to the equation describing the continuity of the time-dependent traction vector through the imperfect interface, one can obtain:

$$\left[\bar{\sigma}_{ij}(s) \right] n_j = \left[\bar{\sigma}_{ij}^{(k+1)}(s) - \bar{\sigma}_{ij}^{(k)}(s) \right] n_j = 0 \tag{2.14}$$

Equations (2.12) and (2.14) show the analogy between the imperfect viscoelastic interface and the elastic one. The role played by $\bar{\Psi}_{ij}(s)$ in viscoelastic problems is the same of Ψ_{ij} played in elastic ones.

IMPERFECT HYBRID HOMOGENIZATION APPROACH

Mori-Tanaka mean field model

The homogenization approach in this work starts with the estimation of the effective behavior of each reinforced layer. This step is decomposed into two parts: the localization part, where the transition scale is made between the averaged local fields and the macroscopic ones based on the solution of the integral equation and Mori-Tanaka’s hypothesis, and then the part where the effective behavior is derived based on averaged techniques. The Mori–Tanaka mean field approach is used in this work because, besides its ease of implementation, it is well known to be accurate. Unlike other micromechanical models, such as the Self-Consistent, the Generalized Self-Consistent, and the Incremental Self-Consistent, the Mori-Tanaka model gives an explicit expression of the effective moduli, which means there is no need for iterative procedures, and it gains in the computational cost.

The integral equation is obtained based on solving the partial differential equation (Eq. (2.7)) for displacement using Green function techniques and some mathematical development. Thus, one can obtain the following integral equation relating the partial local strain to the one of the reference medium by [12, 17]:

$$\bar{\epsilon}_{mn}(x, s) = \bar{\epsilon}_{mn}^0(s) - \int_V \bar{\Gamma}_{mnij}(x - x', s) \delta \bar{C}_{ijkl}(x', s) \bar{\epsilon}_{kl}(x', s) dV' \tag{3.1}$$

where $\bar{\Gamma}_{mnij}(x - x', s)$ is the modified Green tensor associated with the reference medium given by:

$$\bar{\Gamma}_{mnij}(x - x', s) = -\frac{1}{2} \left[\bar{G}_{mi,nj}(x - x', s) + \bar{G}_{ni,mj}(x - x', s) \right] \tag{3.2}$$

where \bar{G} is the Green tensor related to the infinite viscoelastic medium.

$\delta \bar{C}_{ijkl}(x, s)$ is the deviation part, and it is expressed as:

$$\delta \bar{C}_{ijkl}(x, s) = \bar{C}_{ijkl}(x, s) - \bar{C}_{ijkl}^0(x, s) \tag{3.3}$$

Following the same procedure as in [12, 17], which is based on the inclusion problem of Eshelby that considers an inclusion of volume V_I and a relaxation tensor $\bar{C}_{ijkl}^I(s)$ embedded in an infinite medium of relaxation tensor $\bar{C}_{ijkl}^0(s)$, the localization equation is obtained relating the averaged strain in the inclusion with the averaged one of the surrounding medium.

$$\hat{\epsilon}_{mn}^I(s) = \hat{\epsilon}_{mn}^0(s) - \frac{1}{V_I} \bar{T}_{mnij}^{II}(s) \Delta \bar{C}_{ijkl}^I(s) \hat{\epsilon}_{kl}^I(s) \tag{3.4}$$

where $\bar{T}_{mnij}^{II}(s)$ is the viscoelastic interaction tensor. It is a function of the relaxation tensor of the reference medium and the shape of the inclusion, and it is given by

$$\bar{T}_{mnij}^{II}(s) = \iint_{V_I} \bar{\Gamma}_{mnij}(r - r', s) dV' dV \tag{3.5}$$

and

$$\Delta \bar{C}_{ijkl}^I(s) = \bar{C}_{ijkl}^I(s) - \bar{C}_{ijkl}^0(s) \tag{3.6}$$

Equation (3.4) allows one to make the transition between the averaged strain in the inclusion $\hat{\epsilon}_{mn}^I(s)$ and the averaged one in the surrounding medium $\hat{\epsilon}_{mn}^0(s)$:

$$\hat{\epsilon}_{kl}^I(s) = \bar{A}_{klmn}^I(s) \hat{\epsilon}_{mn}^0(s) \tag{3.7}$$

where $\bar{A}_{klmn}^I(s)$ is the dilute localization tensor [12, 17] and it is given by

$$\bar{A}_{klmn}^I(s) = \left[I_{mnkl} + \frac{1}{V_I} \bar{T}_{mnij}^{II}(s) \Delta \bar{C}_{ijkl}^I(s) \right]^{-1} \tag{3.8}$$

At this level, the Mori-Tanaka’s assumptions [17] are considered. The infinite surrounding medium is replaced by a matrix of viscoelastic properties $\bar{C}_{ijkl}^M(s)$. In order to derive the Mori-Tanaka’s localization tensor, $\hat{\epsilon}_{mn}^0(s)$ and $\bar{C}_{ijkl}^0(s)$ in Equation (3.4) are replaced respectively by the averaged strain $\hat{\epsilon}_{mn}^M(s)$ and matrix properties $\bar{C}_{ijkl}^M(s)$, then using the fact that the applied macroscopic strain is given by

$$\bar{E}_{kl}(s) = f^M \hat{\epsilon}_{kl}^M(s) + f^I \hat{\epsilon}_{kl}^I(s) \tag{3.9}$$

where f^I and f^M are volume fractions of inclusion and matrix. By taking into account Mori-Tanaka’s assumptions and taking into consideration Equations (3.9) and (3.4), one can obtain

$$\hat{\epsilon}_{kl}^I(s) = \bar{A}_{klmn}^{I(MT)}(s) \bar{E}_{mn}(s) \tag{3.10}$$

in which The Mori-Tanaka’s localization tensor is given by

$$\bar{A}_{klmn}^{I(MT)}(s) = \left[I_{mnkl} + \frac{f^M}{V_I} \bar{T}_{mnij}^{II}(s) \Delta \bar{C}_{ijkl}^I(s) \right]^{-1} \tag{3.11}$$

with

$$\Delta \bar{C}_{ijkl}^I(s) = \bar{C}_{ijkl}^I(s) - \bar{C}_{ijkl}^M(s) \text{ and } f^M = 1 - f^I$$

Inserting equation (3.10) in the expression of the averaged macroscopic stress over a two-phase composite, as in this work two-phase layers are considered, the effective behavior of two-phase viscoelastic composite is obtained as

$$\bar{C}_{ijkl}^{eff}(s) = \bar{C}_{ijkl}^M(s) + f^I \left(\bar{C}_{ijkl}^I(s) - \bar{C}_{ijkl}^M(s) \right) \bar{A}_{klmn}^{I(MT)}(s) \tag{3.12}$$

Equation (3.12) allows one to predict the effective viscoelastic moduli in the frequency domain for different properties of reinforcement and matrix as well as different geometries of reinforcement. This later is used to estimate the effective behavior of each reinforced layer.

The formulation could be generalized to N-phase composites by considering the averaged macroscopic stress, for N phase composites as

$$\bar{E}(s) = f^M \hat{\epsilon}^M(s) + \sum_{I=2}^N f^I \hat{\epsilon}^I(s) \tag{3.13}$$

Inserting the Mori-Tanaka’s assumption in (Eq.3.7) leads to

$$\hat{\epsilon}_{mn}^I(s) = \bar{A}_{mnkl}^I(s) \hat{\epsilon}_{mn}^M(s) \tag{3.14}$$

in which $\Delta \bar{C}_{ijkl}^I(s) = \bar{C}_{ijkl}^I(s) - \bar{C}_{ijkl}^M(s)$

Based on equations (3.13) and (3.14), it is possible to derive an expression that connects the averaged local strain within the inclusion to the applied macroscopic strain on the entire composite.

$$\hat{\boldsymbol{\varepsilon}}_{sv}^I(\boldsymbol{s}) = \bar{\boldsymbol{A}}_{klsv}^I(\boldsymbol{s}) \left(f^M \boldsymbol{I}_{klmn} + \sum_{I=2}^N f^I \bar{\boldsymbol{A}}_{mnkl}^I(\boldsymbol{s}) \right)^{-1} \bar{\boldsymbol{E}}_{mn}(\boldsymbol{s}) \quad (3.15)$$

Equation (3.15) allows one to derive the formulation of the Mori-Tanaka’s concentration tensor for N-phase viscoelastic composites, one can write

$$\bar{\boldsymbol{A}}_{svmn}^{I(MT)}(\boldsymbol{s}) = \bar{\boldsymbol{A}}_{klsv}^I(\boldsymbol{s}) \left(f^M \boldsymbol{I}_{klmn} + \sum_{I=2}^N f^I \bar{\boldsymbol{A}}_{mnkl}^I(\boldsymbol{s}) \right)^{-1} \quad (3.16)$$

Through the homogenization process, which consist of deriving the averaged macroscopic stress over the N-phase composite and inserting equation (3.16) in it, one can deduce the expression of the effective properties of an N-phase viscoelastic composite as

$$\bar{\boldsymbol{C}}_{ijkl}^{eff}(\boldsymbol{s}) = \bar{\boldsymbol{C}}_{ijkl}^M(\boldsymbol{s}) + \sum_{I=2}^N f^I \left(\bar{\boldsymbol{C}}_{ijmn}^I(\boldsymbol{s}) - \bar{\boldsymbol{C}}_{ijmn}^M(\boldsymbol{s}) \right) \bar{\boldsymbol{A}}_{klmn}^{I(MT)}(\boldsymbol{s}) \quad (3.17)$$

This relationship makes it possible to predict the effective coefficients of an N-phase viscoelastic composite material in the frequency domain, taking into account the diversity of types and shapes of the present phases.

Matrix homogenization method

In this section, the effective behavior of the multi-layered reinforced viscoelastic composites with imperfect interfaces is derived. The reinforced layers are replaced with an equivalent homogeneous layer obtained by the Mori-Tanaka model. A representative volume element (RVE) with a volume V is considered of the composite. The considered composite is described in Figure 1. The linear viscoelastic behavior of the k^{th} layer, in the frequency domain is described by

$$\hat{\boldsymbol{\sigma}}_{ij}^{(k)}(\boldsymbol{s}) = \bar{\boldsymbol{C}}_{ijkl}^{*,(k)}(\boldsymbol{s}) \hat{\boldsymbol{\varepsilon}}_{ij}^{(k)}(\boldsymbol{s}) \quad (3.18)$$

where $\bar{\boldsymbol{C}}^{*,(k)}(\boldsymbol{s})$ represents the effective properties of the k^{th} reinforced layer obtained by the Mori-Tanaka model.

The matrix homogenization procedure ([37-40]) is based on the decomposition of the stress and strain tensors into normal and tangential components and they are given in vector and matrix notation as

$$\hat{\boldsymbol{\sigma}}^{(k)}(\boldsymbol{s}) = \begin{pmatrix} \hat{\boldsymbol{\sigma}}_n^{(k)}(\boldsymbol{s}) \\ \hat{\boldsymbol{\sigma}}_t^{(k)}(\boldsymbol{s}) \end{pmatrix}; \quad \hat{\boldsymbol{\varepsilon}}^{(k)}(\boldsymbol{s}) = \begin{pmatrix} \hat{\boldsymbol{\varepsilon}}_n^{(k)}(\boldsymbol{s}) \\ \hat{\boldsymbol{\varepsilon}}_t^{(k)}(\boldsymbol{s}) \end{pmatrix}; \quad (3.19)$$

$$\bar{\boldsymbol{C}}^{*,(k)}(\boldsymbol{s}) = \begin{pmatrix} \bar{\boldsymbol{C}}_{nn}^{*,(k)}(\boldsymbol{s}) & \bar{\boldsymbol{C}}_{nt}^{*,(k)}(\boldsymbol{s}) \\ \bar{\boldsymbol{C}}_{tn}^{*,(k)}(\boldsymbol{s}) & \bar{\boldsymbol{C}}_{tt}^{*,(k)}(\boldsymbol{s}) \end{pmatrix}.$$

with

$$\hat{\boldsymbol{\sigma}}_n^{(k)}(\boldsymbol{s}) = \begin{bmatrix} \hat{\sigma}_{33}^{(k)}(\boldsymbol{s}) \\ \hat{\sigma}_{23}^{(k)}(\boldsymbol{s}) \\ \hat{\sigma}_{13}^{(k)}(\boldsymbol{s}) \end{bmatrix}; \quad \hat{\boldsymbol{\sigma}}_t^{(k)}(\boldsymbol{s}) = \begin{bmatrix} \hat{\sigma}_{11}^{(k)}(\boldsymbol{s}) \\ \hat{\sigma}_{22}^{(k)}(\boldsymbol{s}) \\ \hat{\sigma}_{12}^{(k)}(\boldsymbol{s}) \end{bmatrix}; \quad (3.20)$$

$$\hat{\boldsymbol{\varepsilon}}_n^{(k)}(\boldsymbol{s}) = \begin{bmatrix} \hat{\varepsilon}_{33}^{(k)}(\boldsymbol{s}) \\ 2\hat{\varepsilon}_{23}^{(k)}(\boldsymbol{s}) \\ 2\hat{\varepsilon}_{13}^{(k)}(\boldsymbol{s}) \end{bmatrix}; \quad \hat{\boldsymbol{\varepsilon}}_t^{(k)}(\boldsymbol{s}) = \begin{bmatrix} \hat{\varepsilon}_{11}^{(k)}(\boldsymbol{s}) \\ \hat{\varepsilon}_{22}^{(k)}(\boldsymbol{s}) \\ 2\hat{\varepsilon}_{12}^{(k)}(\boldsymbol{s}) \end{bmatrix}.$$

Using the vector and matrix decomposition, the constitutive behavior of the k^{th} layer is rewritten as

$$\hat{\sigma}_n^{(k)}(s) = \bar{C}_{nn}^{*(k)}(s) \hat{\epsilon}_n^{(k)}(s) + \bar{C}_{nt}^{*(k)}(s) \hat{\epsilon}_t^{(k)}(s) \tag{3.21}$$

$$\hat{\sigma}_t^{(k)}(s) = \bar{C}_{tn}^{*(k)}(s) \hat{\epsilon}_n^{(k)}(s) + \bar{C}_{tt}^{*(k)}(s) \hat{\epsilon}_t^{(k)}(s) \tag{3.22}$$

in which $\bar{C}_{nn}^{*(k)}(s), \bar{C}_{nt}^{*(k)}(s), \bar{C}_{tn}^{*(k)}(s)$ and $\bar{C}_{tt}^{*(k)}(s)$ are matrix blocs related to the normal and tangential directions:

$$\begin{aligned} \bar{C}_{nn}^{*(k)}(s) &= \begin{pmatrix} \bar{C}_{33}^{*(k)}(s) & \bar{C}_{34}^{*(k)}(s) & \bar{C}_{35}^{*(k)}(s) \\ \bar{C}_{34}^{*(k)}(s) & \bar{C}_{44}^{*(k)}(s) & \bar{C}_{45}^{*(k)}(s) \\ \bar{C}_{35}^{*(k)}(s) & \bar{C}_{45}^{*(k)}(s) & \bar{C}_{55}^{*(k)}(s) \end{pmatrix}, \\ \bar{C}_{nt}^{*(k)}(s) &= \begin{pmatrix} \bar{C}_{13}^{*(k)}(s) & \bar{C}_{23}^{*(k)}(s) & \bar{C}_{36}^{*(k)}(s) \\ \bar{C}_{14}^{*(k)}(s) & \bar{C}_{24}^{*(k)}(s) & \bar{C}_{46}^{*(k)}(s) \\ \bar{C}_{15}^{*(k)}(s) & \bar{C}_{25}^{*(k)}(s) & \bar{C}_{56}^{*(k)}(s) \end{pmatrix}, \\ \bar{C}_{tn}^{*(k)}(s) &= \begin{pmatrix} \bar{C}_{13}^{*(k)}(s) & \bar{C}_{14}^{*(k)}(s) & \bar{C}_{15}^{*(k)}(s) \\ \bar{C}_{23}^{*(k)}(s) & \bar{C}_{24}^{*(k)}(s) & \bar{C}_{25}^{*(k)}(s) \\ \bar{C}_{36}^{*(k)}(s) & \bar{C}_{46}^{*(k)}(s) & \bar{C}_{56}^{*(k)}(s) \end{pmatrix}, \\ \bar{C}_{tt}^{*(k)}(s) &= \begin{pmatrix} \bar{C}_{11}^{*(k)}(s) & \bar{C}_{12}^{*(k)}(s) & \bar{C}_{16}^{*(k)}(s) \\ \bar{C}_{12}^{*(k)}(s) & \bar{C}_{22}^{*(k)}(s) & \bar{C}_{26}^{*(k)}(s) \\ \bar{C}_{16}^{*(k)}(s) & \bar{C}_{26}^{*(k)}(s) & \bar{C}_{66}^{*(k)}(s) \end{pmatrix}. \end{aligned} \tag{3.23}$$

The bloc matrices satisfy the following relationships [37-40]:

$$\bar{C}_{nn}^{*(k)}(s) = (\bar{C}_{nn}^{*(k)}(s))^T, \bar{C}_{tt}^{*(k)}(s) = (\bar{C}_{tt}^{*(k)}(s))^T, \bar{C}_{tn}^{*(k)}(s) = (\bar{C}_{nt}^{*(k)}(s))^T. \tag{3.24}$$

T design matrix transposition. Additionally, due to the positive definiteness property of the Voigt elasticity matrix, it is established that the matrices $\bar{C}_{nn}^{(k)}(s), \bar{C}_{tt}^{(k)}(s)$ are also positive definite.

As in the case of perfect interfaces, the applied normal macroscopic stress is considered equal to the averaged normal one in each layer ($\bar{\Sigma}_n(s) = \hat{\sigma}_n^{(k)}(s)$) and the tangential macroscopic strain is equal to the averaged tangential strain in each layer ($\bar{E}_t(s) = \hat{\epsilon}_t^{(k)}(s)$). These hypotheses are used in the following section in order to derive the effective behavior of the multi-layered viscoelastic composite with imperfect interfaces.

Overall behavior of multi-layered viscoelastic composite with imperfect interfaces

The averaged stress over the volume V of the multi-layered composites is given by:

$$\bar{\Sigma}_{ij}(s) = \frac{1}{V} \int_V \bar{\sigma}_{ij}(s) dV = \sum_{k=1}^N f_k \hat{\sigma}_{ij}^{(k)}(s) \tag{3.25}$$

where $\hat{\sigma}_{ij}^{(k)}(s) = \frac{1}{V_k} \int_{V_k} \bar{\sigma}_{ij}(s) dV_k$ is the averaged stress over the volume of the k^{th} layer of volume V_k

The averaged strain over the volume of the multi-layered composite, taking into account the strain jump, is given by (see Appendix A):

$$\begin{aligned} \bar{\mathbf{E}}_{ij}(\mathbf{s}) &= \frac{1}{V} \int_V \bar{\boldsymbol{\varepsilon}}_{ij}(\mathbf{s}) dV \\ &= \sum_{k=1}^N f_k \hat{\boldsymbol{\varepsilon}}_{ij}^{(k)}(\mathbf{s}) + \frac{1}{2V} \sum_{k=1}^{N-1} \int_{S_k} [\bar{\mathbf{u}}_j(\mathbf{s})] \mathbf{n}_i + [\bar{\mathbf{u}}_i(\mathbf{s})] \mathbf{n}_j dS_k \end{aligned} \quad (3.26)$$

The jump of the displacement across the imperfect interface S_k (situated between the k and $k+1$ layers) is denoted by $[\bar{\mathbf{u}}_i(\mathbf{s})]$ with

$$[\bar{\mathbf{u}}_i(\mathbf{s})] = \bar{\mathbf{u}}_i^{(k+1)}(\mathbf{s})|_{S_k} - \bar{\mathbf{u}}_i^{(k)}(\mathbf{s})|_{S_k} \quad (3.27)$$

So that

$$\begin{aligned} \bar{\mathbf{E}}_{ij}(\mathbf{s}) &= \sum_{k=1}^N f_k \hat{\boldsymbol{\varepsilon}}_{ij}^{(k)}(\mathbf{s}) \\ &+ \frac{1}{2V} \sum_{k=1}^{N-1} \int_{S_k} \left\{ (\bar{\mathbf{u}}_j^{(k+1)}(\mathbf{s}) - \bar{\mathbf{u}}_j^{(k)}(\mathbf{s})) \mathbf{n}_i + (\bar{\mathbf{u}}_i^{(k+1)}(\mathbf{s}) - \bar{\mathbf{u}}_i^{(k)}(\mathbf{s})) \mathbf{n}_j \right\} dS_k \end{aligned} \quad (3.28)$$

where $\hat{\boldsymbol{\varepsilon}}^{(k)}(\mathbf{s})$ is the averaged strain over the volume of the k^{th} layer, given by

$$\hat{\boldsymbol{\varepsilon}}_{ij}^{(k)}(\mathbf{s}) = \frac{1}{V_k} \int_{V_k} \bar{\boldsymbol{\varepsilon}}_{ij}(\mathbf{s}) dV_k \quad (3.29)$$

and $f_k = \frac{V_k}{V}$ is for the volume fraction of the k^{th} layer.

Using matrix vector decomposition, the macroscopic normal and tangential averaged stress over the volume of the multi-layered composite is given by

$$\bar{\boldsymbol{\Sigma}}_n(\mathbf{s}) = \sum_{k=1}^N f_k \hat{\boldsymbol{\sigma}}_n^{(k)}(\mathbf{s}), \quad \bar{\boldsymbol{\Sigma}}_t(\mathbf{s}) = \sum_{k=1}^N f_k \hat{\boldsymbol{\sigma}}_t^{(k)}(\mathbf{s}) \quad (3.30)$$

Equation (3.28), after some mathematical development (see Appendix A), and using matrix vector decomposition, one can derive the expression of the normal and tangential averaged strain over the volume of the multi-layered composite as

$$\bar{\mathbf{E}}_n(\mathbf{s}) = \sum_{k=1}^N f_k \hat{\boldsymbol{\varepsilon}}_n^{(k)}(\mathbf{s}) + \mathbf{h}^{-1} \sum_{k=1}^{N-1} \bar{\boldsymbol{\Gamma}}^{(k)}(\mathbf{s}) \hat{\boldsymbol{\sigma}}_n^{(k)}(\mathbf{s}), \quad (3.31)$$

$$\bar{\mathbf{E}}_t(\mathbf{s}) = \sum_{k=1}^N f_k \hat{\boldsymbol{\varepsilon}}_t^{(k)}(\mathbf{s}) \quad (3.32)$$

where $\bar{\boldsymbol{\Gamma}}^{(k)}(\mathbf{s})$ is the compliance matrix containing the imperfect interface parameters (Appendix A).

From Equation (3.23) and using the fact that $\bar{\boldsymbol{\Sigma}}_n(\mathbf{s}) = \hat{\boldsymbol{\sigma}}_n^{(k)}(\mathbf{s})$ and $\bar{\mathbf{E}}_t(\mathbf{s}) = \hat{\boldsymbol{\varepsilon}}_t^{(k)}(\mathbf{s})$ lead to

$$\begin{aligned} \hat{\boldsymbol{\varepsilon}}_n^{(k)}(\mathbf{s}) &= \left(\bar{\mathbf{C}}_{nn}^{*(k)}(\mathbf{s}) \right)^{-1} \left(\hat{\boldsymbol{\sigma}}_n^{(k)}(\mathbf{s}) - \bar{\mathbf{C}}_{nt}^{*(k)}(\mathbf{s}) \hat{\boldsymbol{\varepsilon}}_t^{(k)}(\mathbf{s}) \right) \\ &= \left(\bar{\mathbf{C}}_{nn}^{*(k)}(\mathbf{s}) \right)^{-1} \left(\bar{\boldsymbol{\Sigma}}_n(\mathbf{s}) - \bar{\mathbf{C}}_{nt}^{*(k)}(\mathbf{s}) \bar{\mathbf{E}}_t(\mathbf{s}) \right) \end{aligned} \quad (3.33)$$

Inserting Equation (3.33) into (3.31), one can write

$$\bar{\mathbf{E}}_n(\mathbf{s}) = \sum_{k=1}^N f_k \left(\bar{\mathbf{C}}_{nn}^{*(k)}(\mathbf{s}) \right)^{-1} \left(\bar{\boldsymbol{\Sigma}}_n(\mathbf{s}) - \bar{\mathbf{C}}_{nt}^{*(k)}(\mathbf{s}) \bar{\mathbf{E}}_t(\mathbf{s}) \right) + \mathbf{h}^{-1} \sum_{k=1}^{N-1} \bar{\boldsymbol{\Gamma}}^{(k)}(\mathbf{s}) \bar{\boldsymbol{\Sigma}}_n(\mathbf{s}) \quad (3.34)$$

Rearranging Equation (3.35) and after some mathematical [40, 44] development leads to

$$\begin{aligned} \bar{\Sigma}_n(s) &= \left[\sum_{k=1}^N f_k \left(\bar{C}_{nn}^{*,(k)}(s) \right)^{-1} + h^{-1} \sum_{k=1}^{N-1} \bar{\Gamma}^{(k)}(s) \right]^{(-1)} \bar{E}_n(s) \\ &+ \left[\sum_{k=1}^N f_k \left(\bar{C}_{nn}^{*,(k)}(s) \right)^{-1} + h^{-1} \sum_{k=1}^{N-1} \bar{\Gamma}^{(k)}(s) \right]^{(-1)} \left[\sum_{k=1}^N f_k \left(\bar{C}_{nn}^{*,(k)}(s) \right)^{-1} \bar{C}_{nt}^{*,(k)}(s) \right] \bar{E}_t(s) \end{aligned} \quad (3.35)$$

Equation (3.35) describes the macroscopic behavior of the multi-layered composites relating the normal stress vector to the normal and tangential strain vectors. The macroscopic behavior has the same form as the local one of each layer, given by:

$$\bar{\Sigma}_n(s) = \bar{C}_{nn}^{eff}(s) \bar{E}_n(s) + \bar{C}_{nt}^{eff}(s) \bar{E}_t(s) \quad (3.36)$$

From Equations (3.36) and (3.35), one can write

$$\bar{C}_{nn}^{eff}(s) = \left[\sum_{k=1}^N f_k \left(\bar{C}_{nn}^{*,(k)}(s) \right)^{-1} + h^{-1} \sum_{k=1}^{N-1} \bar{\Gamma}^{(k)}(s) \right]^{-1} \quad (3.37)$$

$$\bar{C}_{nt}^{eff}(s) = \bar{C}_{nn}^{eff}(s) \left[\sum_{k=1}^N f_k \left(\bar{C}_{nn}^{*,(k)}(s) \right)^{-1} \bar{C}_{nt}^{*,(k)}(s) \right] \quad (3.38)$$

To complete the determination of the effective behavior, $\bar{C}_{nn}^{eff}(s)$ and $\bar{C}_{nt}^{eff}(s)$, one has to substitute Equation (3.21) into (3.22):

$$\hat{\sigma}_t^{(k)}(s) = \bar{C}_{tn}^{*,(k)}(s) \left(\bar{C}_{nn}^{*,(k)}(s) \right)^{-1} \left(\bar{\Sigma}_n(s) - \bar{C}_{nt}^{*,(k)}(s) \bar{E}_t(s) \right) + \bar{C}_{tt}^{*,(k)}(s) \bar{E}_t(s) \quad (3.39)$$

Rearranging Equation (3.39) and using (3.30) leads to:

$$\begin{aligned} \bar{\Sigma}_t(s) &= \sum_{k=1}^N f_k \bar{C}_{tn}^{*,(k)}(s) \left(\bar{C}_{nn}^{*,(k)}(s) \right)^{-1} \bar{\Sigma}_n(s) \\ &+ \sum_{k=1}^N f_k \left[\bar{C}_{tt}^{*,(k)}(s) - \bar{C}_{tn}^{*,(k)}(s) \left(\bar{C}_{nn}^{*,(k)}(s) \right)^{-1} \bar{C}_{nt}^{*,(k)}(s) \right] \bar{E}_t(s) \end{aligned} \quad (3.40)$$

Substituting Equation (3.36) into (3.40) gives

$$\begin{aligned} \bar{\Sigma}_t(s) &= \left[\sum_{k=1}^N f_k \bar{C}_{tn}^{*,(k)}(s) \left(\bar{C}_{nn}^{*,(k)}(s) \right)^{-1} \right] \bar{C}_{nn}^{eff}(s) \bar{E}_n(s) \\ &+ \left[\sum_{k=1}^N f_k \bar{C}_{tt}^{*,(k)}(s) + \sum_{k=1}^N f_k \bar{C}_{tn}^{*,(k)}(s) \left(\bar{C}_{nn}^{*,(k)}(s) \right)^{-1} \left(\bar{C}_{nt}^{eff}(s) - \bar{C}_{nt}^{*,(k)}(s) \right) \right] \bar{E}_t(s) \end{aligned} \quad (3.41)$$

The macroscopic behavior given by the tangential stress vector:

$$\bar{\Sigma}_t(s) = \bar{C}_{tn}^{eff}(s) \bar{E}_n(s) + \bar{C}_{tt}^{eff}(s) \bar{E}_t(s) \quad (3.42)$$

Comparing Equation (3.41) with (3.42) leads to the expression of the effective behavior given by

$$\bar{C}_{tn}^{eff}(s) = \left[\sum_{k=1}^N f_k \left(\bar{C}_{nn}^{*,(k)}(s) \right)^{-1} \bar{C}_{nt}^{*,(k)}(s) \right] \bar{C}_{nn}^{eff}(s) \quad (3.43)$$

$$\bar{C}_{tt}^{eff}(s) = \sum_{k=1}^N f_k \bar{C}_{tt}^{*,(k)}(s) + \sum_{k=1}^N f_k \bar{C}_{tn}^{*,(k)}(s) \left(\bar{C}_{nn}^{*,(k)}(s) \right)^{-1} \left(\bar{C}_{nt}^{eff}(s) - \bar{C}_{nt}^{*,(k)}(s) \right) \quad (3.44)$$

The effective behavior of the multi-layered reinforced viscoelastic composites with imperfect interfaces is completely estimated by

$$\left\{ \begin{aligned} \bar{C}_{nn}^{eff}(s) &= \left[\sum_{k=1}^N f_k \left(\bar{C}_{nn}^{*,(k)}(s) \right)^{-1} + h^{-1} \sum_{k=1}^{N-1} \Gamma^{(k)}(s) \right]^{-1}, \\ \bar{C}_{nt}^{eff}(s) &= \bar{C}_{nn}^{eff}(s) \left[\sum_{k=1}^N f_k \left(\bar{C}_{nn}^{*,(k)}(s) \right)^{-1} \bar{C}_{nt}^{*,(k)}(s) \right], \\ \bar{C}_{tn}^{eff}(s) &= \left(\bar{C}_{nt}^{eff}(s) \right)^T, \\ \bar{C}_{tt}^{eff}(s) &= \sum_{k=1}^N f_k \bar{C}_{tt}^{*,(k)}(s) + \sum_{k=1}^N f_k \bar{C}_{tn}^{*,(k)}(s) \left(\bar{C}_{nn}^{*,(k)}(s) \right)^{-1} \left(\bar{C}_{nt}^{eff}(s) - \bar{C}_{nt}^{*,(k)}(s) \right). \end{aligned} \right. \quad (3.45)$$

$\bar{C}_{nn}^{*,(k)}(s), \bar{C}_{nt}^{*,(k)}(s), \bar{C}_{tn}^{*,(k)}(s)$ and $\bar{C}_{tt}^{*,(k)}(s)$ represent the local behavior of the k^{th} reinforced layer estimated by the Mori-Tanaka model. The relaxation effective matrix $\bar{C}^{eff}(s)$, constituted with the four matrix blocs $\bar{C}_{nn}^{*,(k)}(s), \bar{C}_{nt}^{*,(k)}(s), \bar{C}_{tn}^{*,(k)}(s)$ and $\bar{C}_{tt}^{*,(k)}(s)$, is a complex matrix given by:

$$\bar{C}^{eff}(s) = \bar{C}_R^{eff}(s) + i \bar{C}_I^{eff}(s) \quad (3.46)$$

such as $\bar{C}_R^{eff}(s)$ is the real part (storage part) and $\bar{C}_I^{eff}(s)$ the imaginary part (loss part).

TIME-DEPENDENT BEHAVIOR OF THE MULTI-LAYERED VISCOELASTIC COMPOSITE

In the previous section (Section 3), the effective viscoelastic behavior of multi-layered composites is derived in the frequency domain. That is allowing one to estimate the frequency-dependent behavior. In this section, the effective behavior will be inverted, numerically, based on the inverse of the Laplace-Carson transform. The analytical inverse of the Laplace-Carson transform of the effective behavior to the time domain is expressed as

$$C_{mjkl}^{eff}(t) = \frac{1}{2\pi i} \int_B \frac{\bar{C}_{mjkl}^{eff}(s)}{s} \exp(ts) ds \quad (4.1)$$

where B is the Bromwich contour (See Reference [45] for definition).

The analytical evaluation of Equation (4.1) is impossible due to the implicit dependence of $\bar{C}_{mjkl}^{eff}(s)$ on the Carson variable s . In this paper, the inversion is performed numerically. Many algorithms have been developed to compute the numerical inversion of the Laplace-Carson transform. The Talbot algorithm is used in this work [45], which allows one to express the time-dependent behavior of the considered multi-layered composite as:

$$C_{mjkl}^{eff}(t, M) = \frac{r}{M} \left[\frac{1}{2} \bar{C}_{mjkl}^{eff}(r) \exp(rt) + \sum_{k=1}^{M-1} Re \left[\exp(ts(\theta_k)) \bar{C}_{mjkl}^{eff}(s(\theta_k)) (1 + i\chi(\theta_k)) \right] \right] \quad (4.2)$$

with $r = \frac{2M}{5t}$, $\theta_k = \frac{k\pi}{M}$,

$$\chi(\theta_k) = \theta_k + \theta_k (\cot(\theta_k) - 1) \cot(\theta_k) \text{ and } s(\theta_k) = r\theta_k (\cot(\theta_k) + i)$$

The precision of the inversion to the time domain given by Equation (4.2) depends on the free parameter M, which indicates the number of additions to perform. Based on Equation (4.2), the effective behavior is predicted in the time domain taking into account the properties of each reinforced layer (estimated by the Mori-Tanaka model), volume fractions of layers, and the imperfect interface parameters. The fixed Talbot algorithm used in this work was already used in [25-27] to make the inversion of the effective behavior of viscoelastic composites from the frequency to the time domain, and it is validated by comparison with a developed straightforward formalism in the time domain.

NUMERICAL RESULTS

In this section, the numerical implementation of the developed model is performed in order to estimate the effective viscoelastic behavior of multi-layered composites with imperfect viscoelastic interfaces. The prediction is done first in the frequency domain, then in the time one. Two kinds of composites are considered: a two-layer composite and a three-layered one. The viscoelastic properties of imperfect interfaces are considered to follow the Maxwell’s model. Each layer is reinforced with aligned fibers in the x_2 direction. The homogenization of the reinforced layers is done using the Mori-Tanaka model. The expression of effective properties obtained by the Mori-Tanaka model (Eq. (3.12)) is for the general case of ellipsoidal inclusion. In the implementation, ellipsoidal inclusions of semi-axes a , b , and c aligned with directions x_1 , x_2 , and x_3 , respectively, are considered. In order to obtain aligned fibers in the x_2 direction, the semi-axes are taken ($a = 1$, $b = 1000$, $c = 1$).

Two-layered viscoelastic composite

Frequency domain

The two-layered composite (Fig. 5) is constituted of two layers separated by an imperfect interface, which has the viscoelastic properties described by the Maxwell’s model (Eq. (5.1)). The two layers are constituted with carbon fibers (properties are listed in table 1) embedded in a viscoelastic matrix where the behavior is described by the Burger’s model (Eq. (5.2)). Since the two layers have the same constituents, one can see the considered configuration as a single layer with a single imperfect interface.

The expressions for the creep compliance in Burger’s and Maxwell’s models are given, respectively, as follows (see [44]).

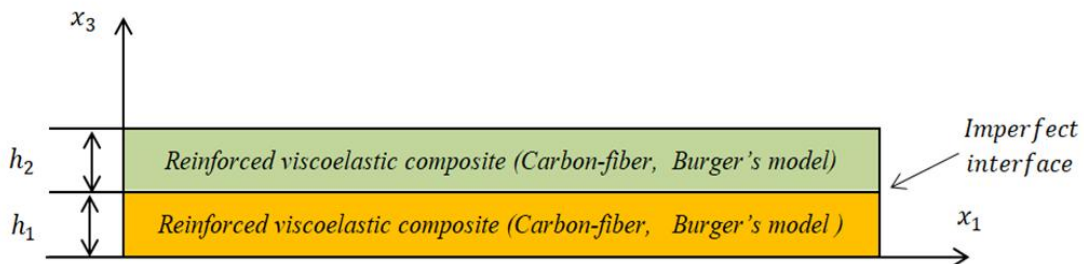


Figure 5. Two-layered viscoelastic composite for the imperfect hybrid model

Table 1. Parameters for elastic materials

Parameter	E (GPa)	ν
Carbon fiber	235	0.3
Epoxy	5	0.4

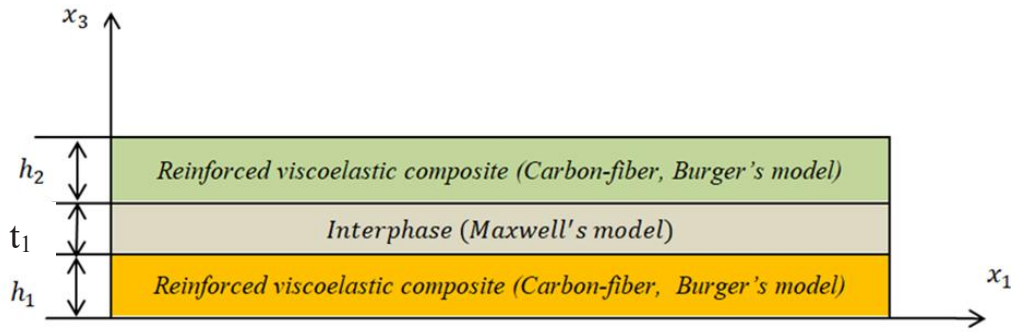


Figure 6. Two-layered viscoelastic composite for the perfect hybrid model

$$S_{Burger}(t) = \frac{1}{E_0} + \frac{1}{E_1} \left(1 - \exp\left(\frac{E_1 t}{\eta_1}\right) \right) + \frac{t}{\eta_2}, \tag{5.1}$$

$$S_{Maxwell}(t) = \frac{1}{E_0} + \frac{t}{\eta_0}. \tag{5.2}$$

Applying the Carson-Laplace transform on Equations (5.1) and (5.2), gives

$$\bar{S}_{Burger}(s) = s \left(\frac{1}{sE_0} + \frac{1}{E_1} \left(\frac{1}{s} - \left(\frac{1}{\left(s + \frac{E_1}{\eta_1} \right)} \right) \right) + \frac{1}{s^2 \eta_2} \right), \tag{5.3}$$

$$\bar{S}_{Maxwell}(s) = s \left(\frac{1}{sE_0} + \frac{1}{s^2 \eta_0} \right). \tag{5.4}$$

One can deduce the Young's modulus by

$$\bar{E}_{Burger}(s) = \frac{1}{\bar{S}_{Burger}(s)}, \tag{5.5}$$

$$\bar{E}_{Maxwell}(s) = \frac{1}{\bar{S}_{Maxwell}(s)}. \tag{5.6}$$

Poisson's ratio of the used viscoelastic materials is taken as constant and they are listed in Table 2.

The imperfect interface parameters are obtained using the following relationships [44, 48].

$$\bar{\alpha}(s) = \frac{t_1}{\bar{\mu}_c(s)}, \quad \bar{\beta}(s) = \frac{t_1}{(\bar{\lambda}_c(s) + 2\bar{\mu}_c(s))}. \tag{5.7}$$

where t_1 is the thickness of the interface.

with

$$\bar{\mu}_c(s) = \frac{\bar{E}_{Maxwell}(s)}{2(1 + \bar{\nu}(s))}, \quad \bar{\lambda}_c(s) = \frac{\bar{E}_{Maxwell}(s)\bar{\nu}(s)}{(1 + \bar{\nu}(s))(1 - 2\bar{\nu}(s))}. \tag{5.8}$$

Table 2. Parameters for viscoelastic materials [44]

Parameter	E_0 (GPa)	E_1 (GPa)	η_0 (GPa·h)	η_1 (GPa·h)	η_2 (GPa·h)	ν
Maxwell's model	2.5	-	50	-	-	0.25
Burger's model	2.5	1.8	-	300	8000	0.25

For the homogenization of each layer with The Mori-Tanaka model, the volume fraction of the viscoelastic matrix is fixed at $f_M = 0.64$. The total thickness of the two-phase multi-layered composite is set at $h = 3 \times 10^{-1}$ m. The volume fraction of the first layer is fixed at 0.35.

For the sake of comparison and validation of the developed formalism, two other models are considered. One model is called the perfect hybrid model, and it is constituted by considering the imperfect interface as an interlayer (Fig. 6) of thickness t_1 ($t_1 = 3 \times 10^{-3}$) situated between the first and the second layer where the interfaces are perfect. That way, one finds a three-layered composite constituted of the first layer, interlayer, and the second layer where interfaces are perfectly bounded. The effective properties of the three-layered viscoelastic composite are predicted based on Equation (3.45), where the terms due to the imperfect interphase are neglected. The volume fractions of each layer are taken as $f_3 = 0.64$ (second layer), $f_2 = t_1/h$ (interphase) and $f_1 = 1 - f_2 - f_3$ (first layer).

The numerical results are presented based on the two models: imperfect hybrid model and perfect hybrid model in the frequency domain. It is shown, in Figures 7a – 7f, the variation of the storage and loss part of effective moduli $\bar{C}_{11}^{eff}, \bar{C}_{22}^{eff}, \bar{C}_{33}^{eff}, \bar{C}_{12}^{eff}, \bar{C}_{13}^{eff}$ and \bar{C}_{66}^{eff} , respectively. It is clearly demonstrated that the two proposed models predict the same results. The loss part of effective moduli shows the dissipation's characteristic of the composite, and the storage part shows the stiffness of the composite. In all the figures, the numerical results are presented with the reference case ($t_1 = 0$), and one can see the influence of the imperfect interface on the numerical estimation. One can also remark that the obtained effective behavior, in the case of $t_1 = 0$, is transversally isotropic ($\bar{C}_{11}^{eff} = \bar{C}_{33}^{eff} \neq \bar{C}_{22}^{eff}$) and this is due to the fact that the two layers are the same and to the reinforcement direction. But, when the imperfect interface is considered, one can remark that \bar{C}_{11}^{eff} is slightly different to \bar{C}_{33}^{eff} , which is explained by the fact that the imperfect interface introduces an isotropy in x_3 direction. It is clear

that with a proper choice of materials, one can design multi-layer composites with high dissipation characteristics.

Time domain

In this section, the effective properties are presented in the time domain for the same two-layered composites considered in the frequency domain. The effective properties are predicted based on the imperfect hybrid model, perfect hybrid mode and coated model. The inversion from the frequency domain to the time one is done based on the fixed Talbot algorithm. The free parameter M is taken equal to 10, as explained in [27]; when M = 10, the fixed Talbot algorithm gives good precision.

To analyze the dependence of the CPU time on the M parameter of the Talbot algorithm, the CPU time is computed with respect to M (see Appendix B). One can see that the CPU time increases as the parameter M, which is the number of summations, increases.

In Figures 8a – 8f, the effective moduli $C_{11}^{eff}, C_{22}^{eff}, C_{33}^{eff}, C_{12}^{eff}, C_{13}^{eff}$ and C_{66}^{eff} are presented with respect to the time variable based on the two considered models. It is clearly shown that the three models predict superimposed predictions. The relaxation behavior of the composite is shown on the presented effective moduli. In all the figures, results are presented with the reference case ($t_1 = 0$). The effect of the imperfect interface is clearly shown in the results. Again, as in the frequency domain, one can see that $C_{11}^{eff} = C_{22}^{eff} \neq C_{33}^{eff}$ in the case of $t_1 = 0$, and when the imperfect interface effect is considered, it remarked that C_{11}^{eff} is slightly different to C_{22}^{eff} .

In order to present the elliptical cycles due to harmonic strains applied on the composite, the considered two-layered composite is subjected to a uniaxial strain:

$$\epsilon_{11}(t) = \epsilon_{11}^{\max} \exp(i\omega t) \quad (5.10)$$

with $\epsilon_{11}^{\max} = 1$.

One can write the following relationship between the stress and strain:

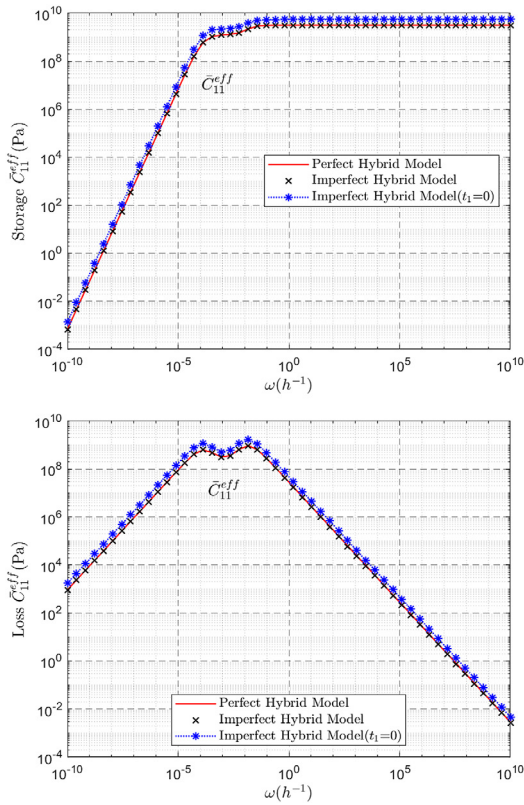


Figure 7a. Storage and loss parts of the effective viscoelastic modulus \bar{C}_{11}^{eff} of the two-layered viscoelastic composite with an imperfect interface

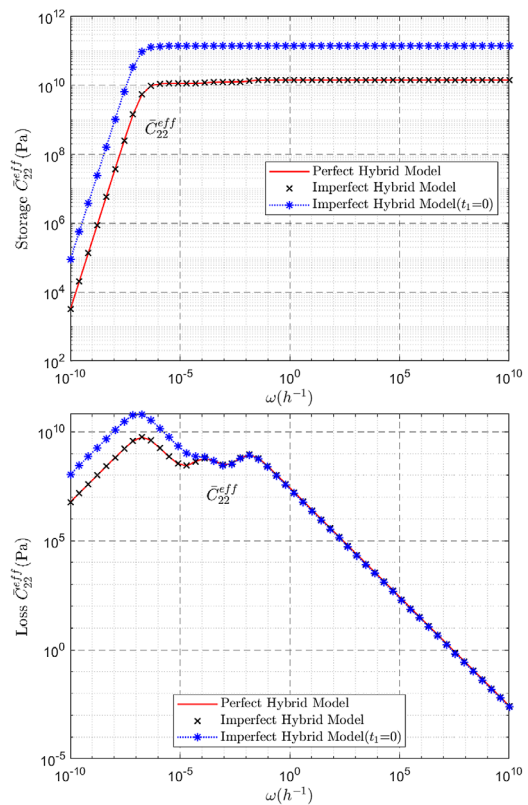


Figure 7b. Storage and loss parts of the effective viscoelastic modulus \bar{C}_{22}^{eff} of the two-layered viscoelastic composite with an imperfect interface

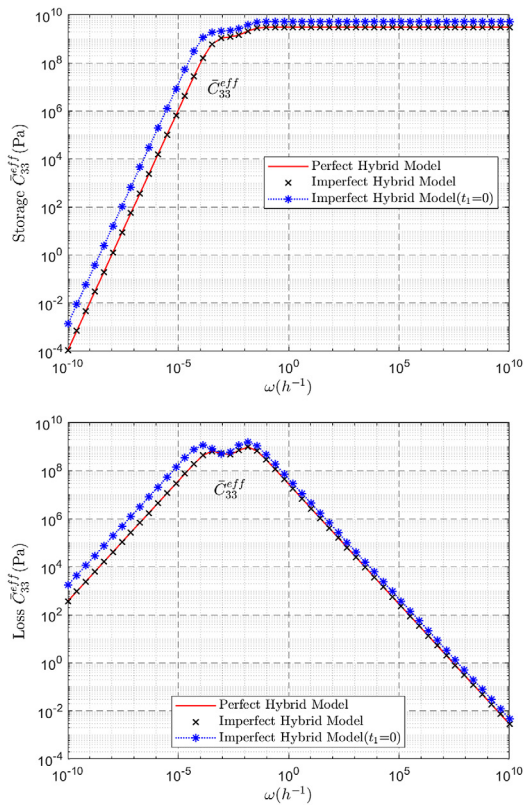


Figure 7c. Storage and loss parts of the effective viscoelastic modulus \bar{C}_{33}^{eff} of the two-layered viscoelastic composite with an imperfect interface

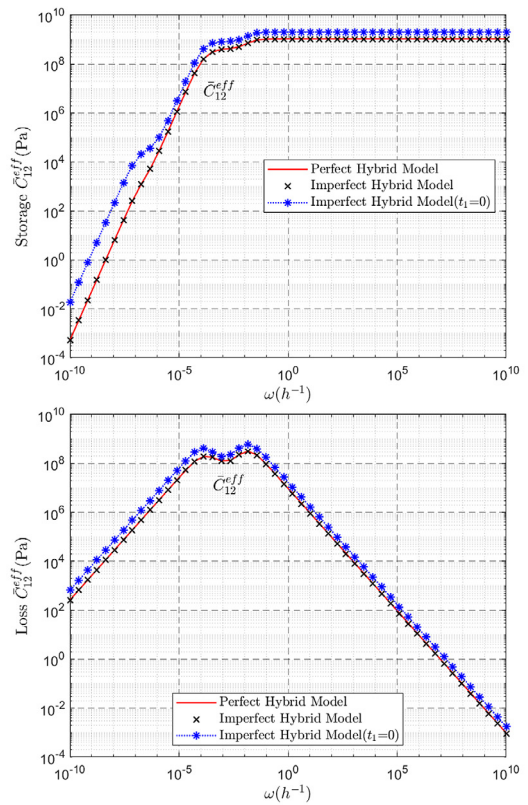


Figure 7d. Storage and loss parts of the effective viscoelastic modulus \bar{C}_{12}^{eff} of the two-layered viscoelastic composite with an imperfect interface

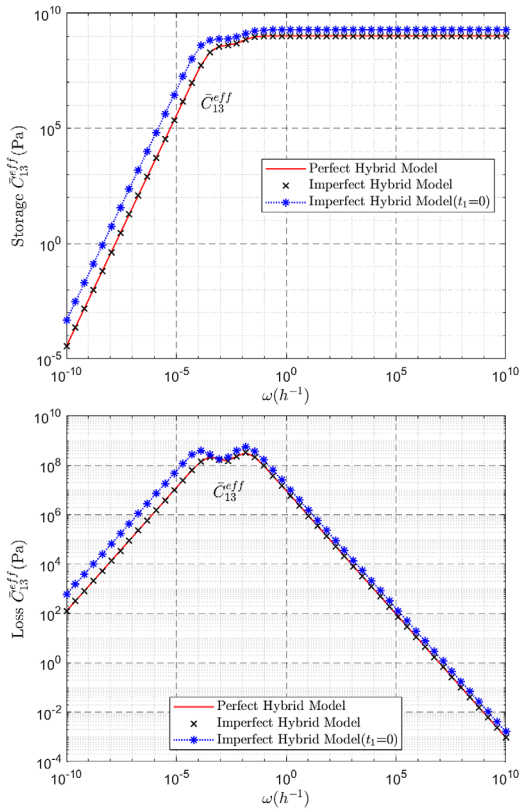


Figure 7e. Storage and loss parts of the effective viscoelastic modulus \bar{C}_{13}^{eff} of the two-layered viscoelastic composite with an imperfect interface

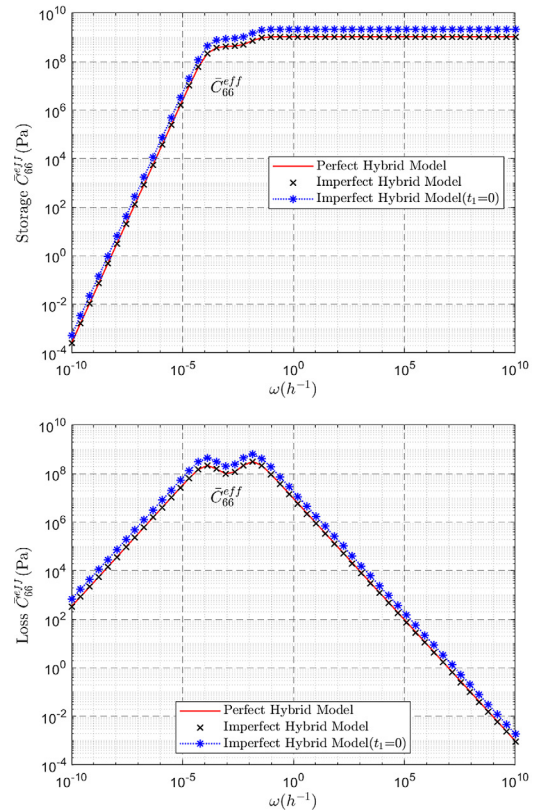


Figure 7f. Storage and loss parts of the effective viscoelastic modulus \bar{C}_{66}^{eff} of the two-layered viscoelastic composite with an imperfect interface

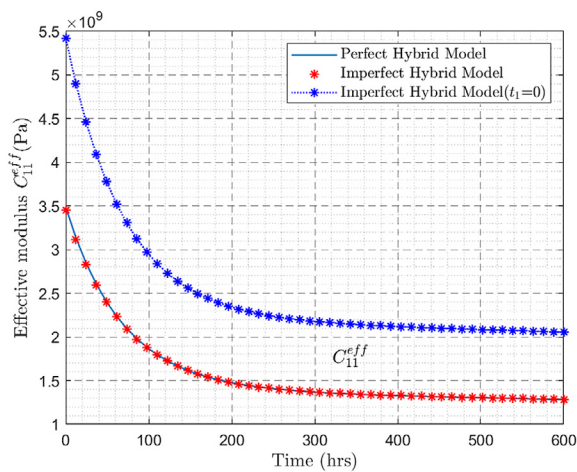


Figure 8a. Effective viscoelastic modulus C_{11}^{eff} for the two-layered viscoelastic composite with an imperfect interface

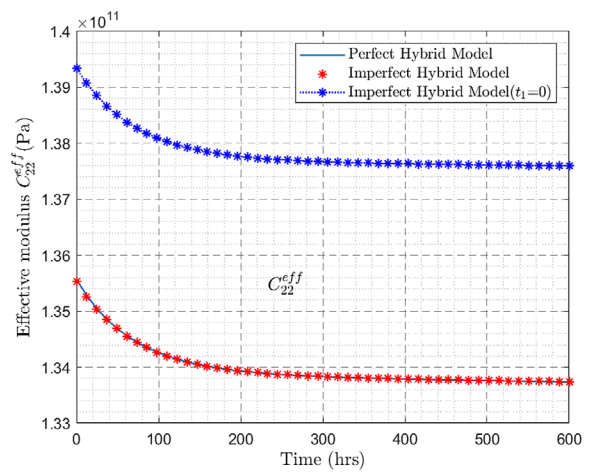


Figure 8b. Effective viscoelastic modulus C_{22}^{eff} for the two-layered viscoelastic composite with an imperfect interface

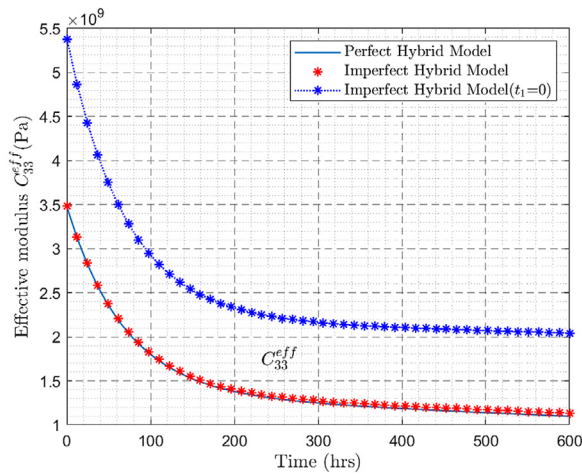


Figure 8c. Effective viscoelastic modulus C_{33}^{eff} for the two-layered viscoelastic composite with an imperfect interface

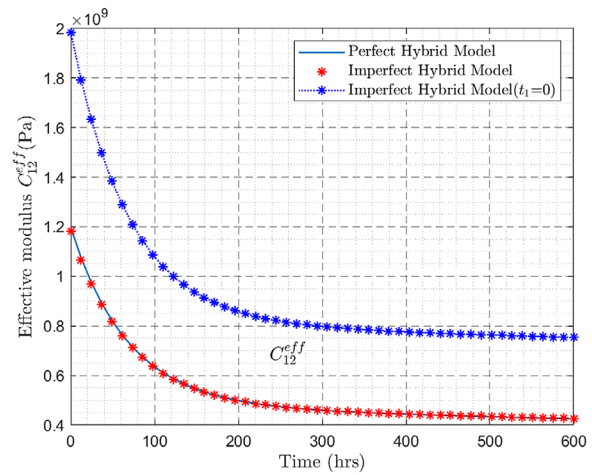


Figure 8d. Effective viscoelastic modulus C_{12}^{eff} for the two-layered viscoelastic composite with an imperfect interface

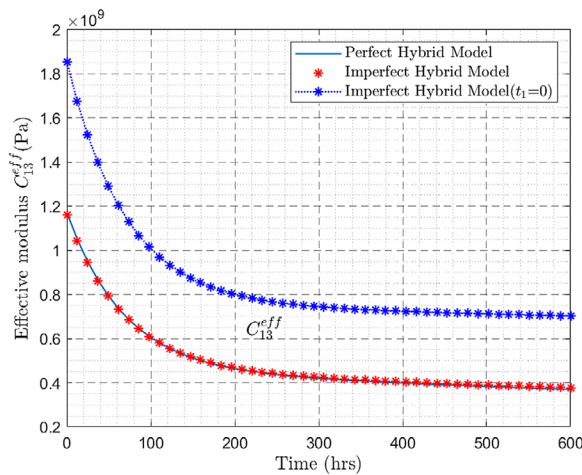


Figure 8e. Effective viscoelastic modulus C_{13}^{eff} for the two-layered viscoelastic composite with an imperfect interface

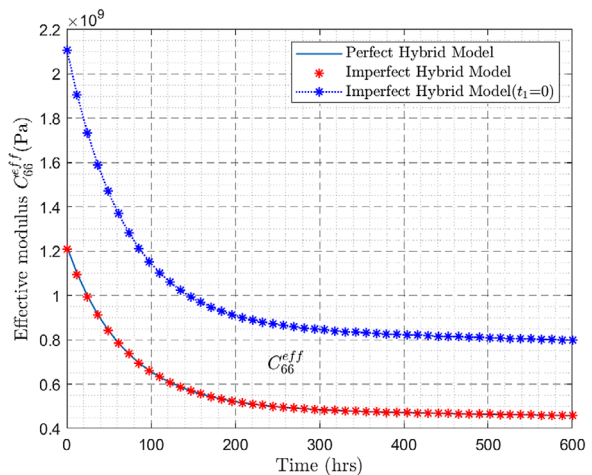


Figure 8f. Effective viscoelastic modulus C_{66}^{eff} for the two-layered viscoelastic composite with an imperfect interface

$$\sigma_{11}(t) = \text{Re}(\bar{C}_{11}^{eff}(s)\epsilon_{11}^{\max} \exp(i\omega t)) \quad (5.11)$$

where $\bar{C}_{11}^{eff}(s)$ is the effective viscoelastic modulus of the composite.

The elliptical cycles (normalized stress/strain) are presented in Figure 9 for the considered two-layered viscoelastic composite based on the imperfect hybrid model. The effect of frequencies on the hysteretic response of the composite material is clearly shown. One can see that the smaller the frequency, the bigger the elliptical cycle is. That is explained by the fact that the attenuation factor increases as the frequency decreases. Also, the area of elliptical cycles shows the dissipated energy due to a harmonic force, which demonstrates the damping capability of composites.

Three-layered viscoelastic composite

Many composites, for example sandwich composites, used in the industry, are three-layer composites. To show the capability of the model to design and estimate the effective behavior of this kind of composite, a three-layered viscoelastic composite with imperfect interfaces is considered (Fig. 10). The first layer of thickness h_1 is constituted of an epoxy matrix reinforced by aligned carbon fibers in the x_2 direction, the second layer of thickness h_2 is viscoelastic, and its behavior is described by the Burger’s model and the third layer, of thickness h_3 , has material constitutions that are the same as the first layer. Since the first and the third layers are identical and they compose together one layer of thickness

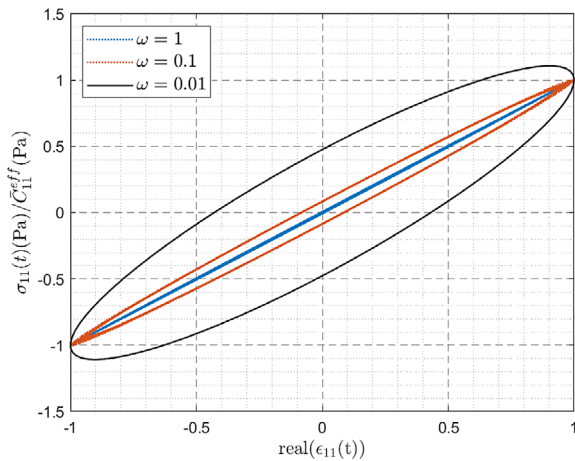


Figure 9. Elliptical cycle (normalized stress/strain) for the two-layered viscoelastic composites with imperfect interface

$h_1 + h_3$, one can see the considered configuration of the composite as a two-layered composite with an imperfect interface between them.

The imperfect interface properties are described by the Maxwell’s model. The effective properties are predicted by the developed Imperfect hybrid formulation. The prediction are compared to the ones obtained by the perfect hybrid model (Fig. 11) where the imperfect interfaces are considered as interphases of thicknesses t_2 and t_3 and their viscoelastic behavior is described by the Maxwell’s model.

For the imperfect hybrid model, the volume fraction of the first layer is taken as $f_1 = 0.175$, second layer is $f_2 = 0.64$ and the third layer is $f_3 = f_1$.

For the perfect hybrid model the following parameters are considered: $t_2 = t_3 = 1.5 \times 10^{-3}$ m, the volume fraction of the first layer is $f_1 = 0.175$, volume fraction of the first interphase $f_2 = t_2/h$, volume fraction of the second layer is $f_3 = 0.64$, volume fraction of the second interphase is $f_4 = t_3/h$ and the volume fraction of the third interphase is $f_5 = 0.175$. The total thickness of the multi-layered composite is $h = 3 \times 10^{-1}$ m.

Frequency domain

Storage and loss parts of the effective viscoelastic moduli \bar{C}_{11}^{eff} , \bar{C}_{22}^{eff} , \bar{C}_{12}^{eff} and \bar{C}_{66}^{eff} are presented in Figures 12a – 12d. Again, it is observed that coefficients predicted by the presented imperfect hybrid model are in good agreement with those predicted by the equivalent perfect hybrid model. All the numerical results are presented with the reference case ($t_2 = t_3 = 0$), and the effect of imperfect interfaces is shown of the effective behavior. Again as in the case of two-layered composites the variation of the storage and loss part with different range of frequencies shows the dissipation and the stiffness characteristics of the considered composites.

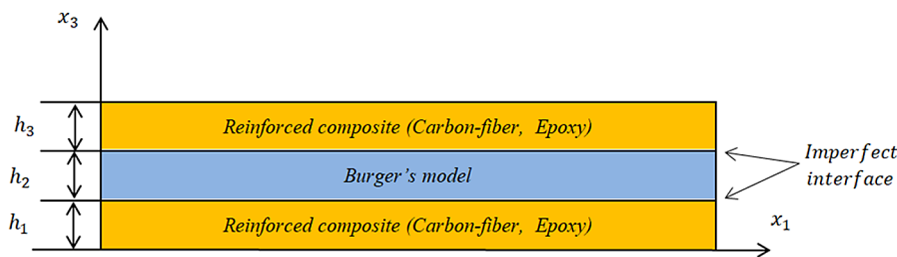


Figure 10. Three-layered viscoelastic composite with imperfect interfaces for the imperfect hybrid model

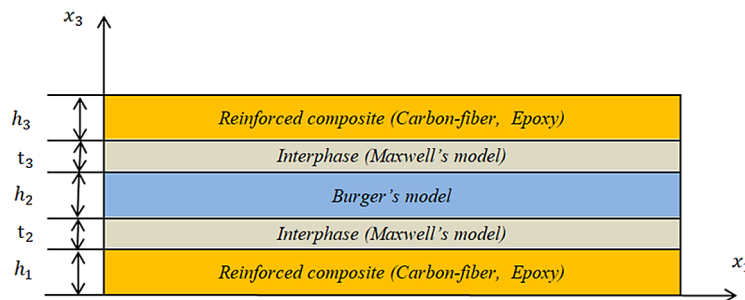


Figure 11. The equivalent viscoelastic composite with the introduced interphases for the perfect hybrid model

Time domain

The effective moduli $C_{11}^{eff}, C_{22}^{eff}, C_{33}^{eff}, C_{12}^{eff}, C_{44}^{eff}$ and C_{66}^{eff} are presented in Figures 13a – 13f in the time domain for the same considered three-layered composite. Again, it is seen that the perfect hybrid model and the imperfect hybrid one predict the same results. It is clearly seen that the resulting behavior is anisotropic ($C_{11}^{eff} \neq C_{22}^{eff} \neq C_{33}^{eff}$). In Figure 14, based on the imperfect hybrid model, the effective modulus C_{11}^{eff} is presented for different thicknesses of the imperfect interfaces. The imperfect sliding and debonding parameters of the imperfect interface vary with the thickness of the interface, and this variation is clearly shown on the presented effective moduli. It is seen that there is a degradation of the effective coefficients as the thickness of the interfaces increases, and this remark is consistent with the mathematical expression presented in Equation

(3.45). The imperfect interface parameters have an effect on the stiffness and the dissipation characteristics of the composites. Also, one can see the relaxation behavior of the composite in the presented effective moduli, which shows the damping capabilities of the considered viscoelastic composites.

CONCLUSIONS

In this work, a hybrid homogenization strategy combining the Mori-Tanaka mean field model with a matrix formulation is developed to predict the frequency and time-dependent behavior of viscoelastic multi-layered composites. Each layer is reinforced with aligned fibers, and the interfaces located between layers are considered imperfect. The linear spring model for elastic imperfect interfaces is generalized to the case of viscoelastic imperfect

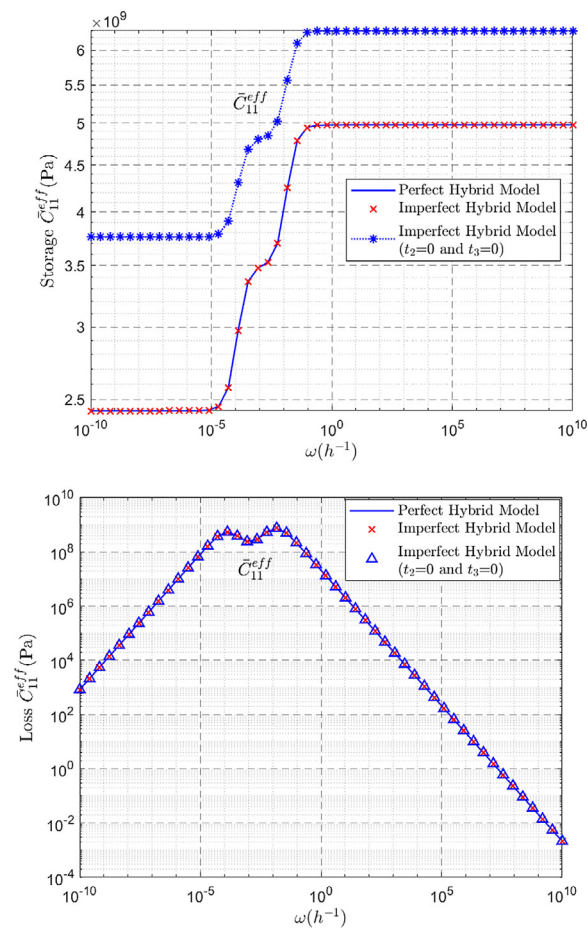


Figure 12a. Storage and loss parts of effective viscoelastic modulus \bar{C}_{11}^{eff} for the three-layered viscoelastic composite with imperfect interfaces

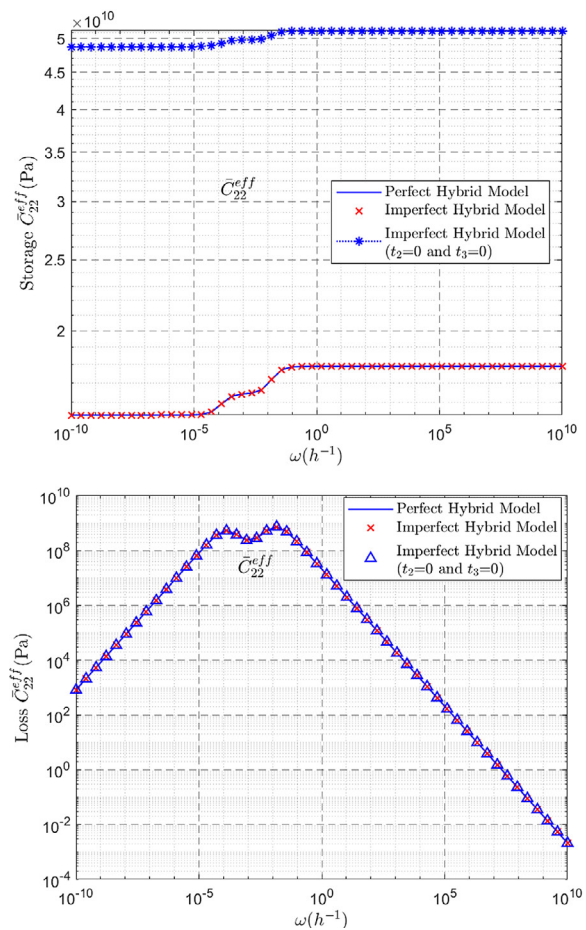


Figure 12b. Storage and loss parts of effective viscoelastic modulus \bar{C}_{22}^{eff} for the three-layered viscoelastic composite with imperfect interfaces

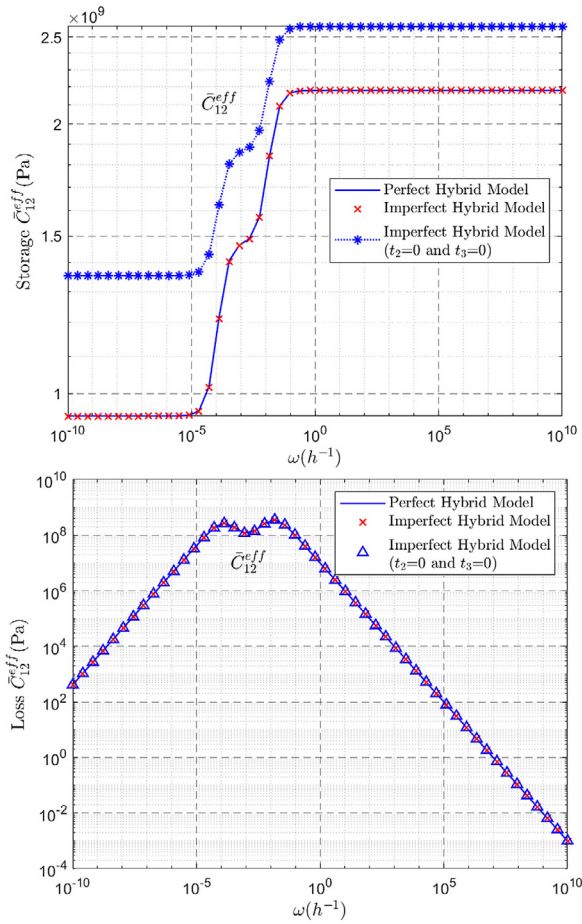


Figure 12c. Storage and loss parts of effective viscoelastic modulus \bar{C}_{12}^{eff} for the three-layered viscoelastic composite with imperfect interfaces

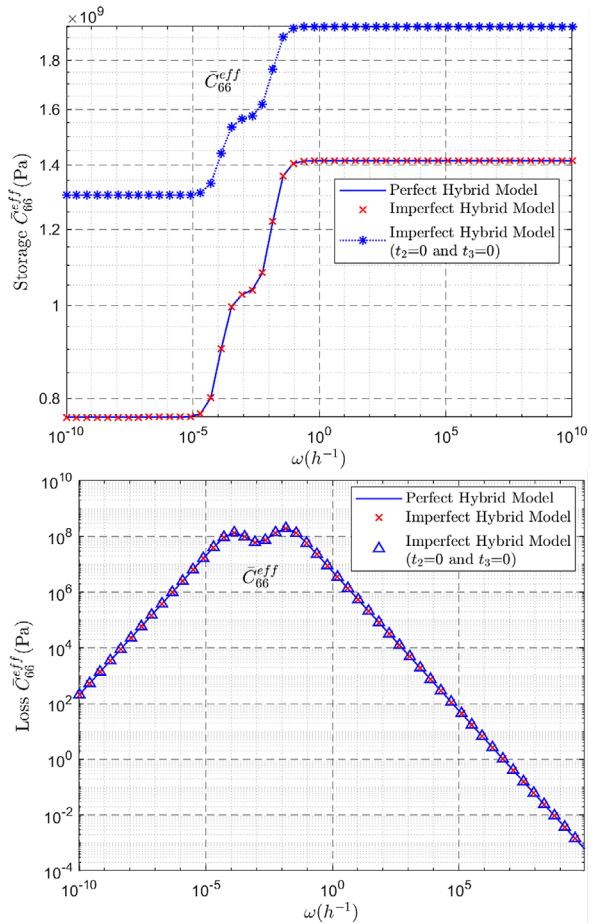


Figure 12d. Storage and loss parts of effective viscoelastic modulus \bar{C}_{66}^{eff} for the three-layered viscoelastic composite with imperfect interfaces

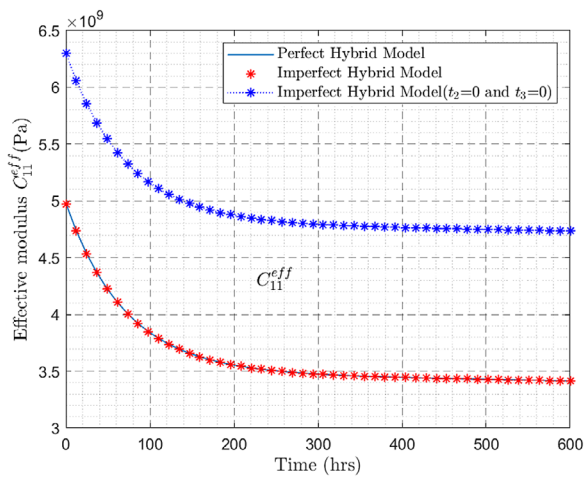


Figure 13a. Time dependent effective viscoelastic modulus C_{11}^{eff} for the three-layered viscoelastic composite with imperfect interfaces

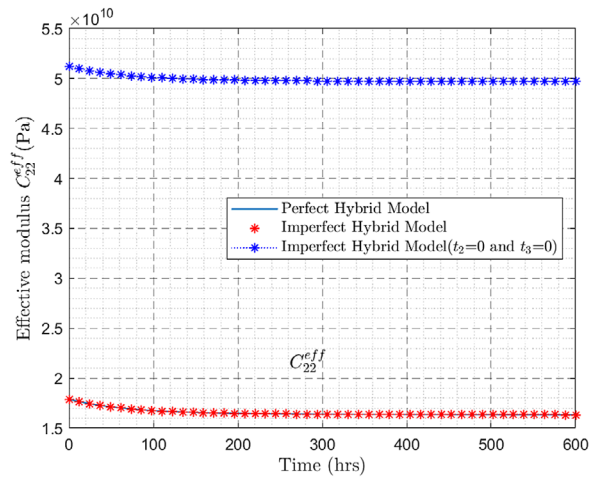


Figure 13b. Time dependent effective viscoelastic modulus C_{22}^{eff} for the three-layered viscoelastic composite with imperfect interfaces

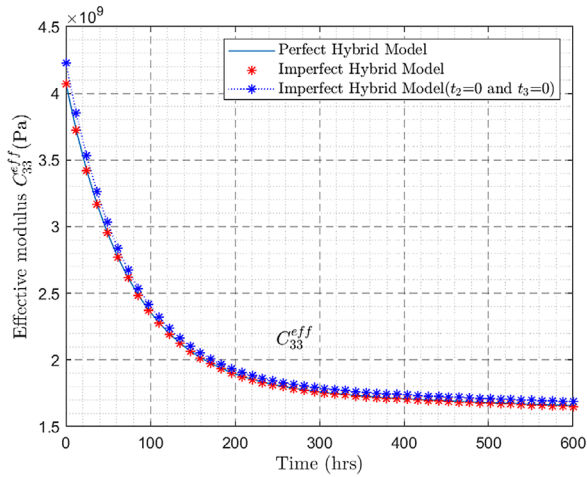


Figure 13c. Time dependent effective viscoelastic modulus C_{33}^{eff} for the three-layered viscoelastic composite with imperfect interfaces

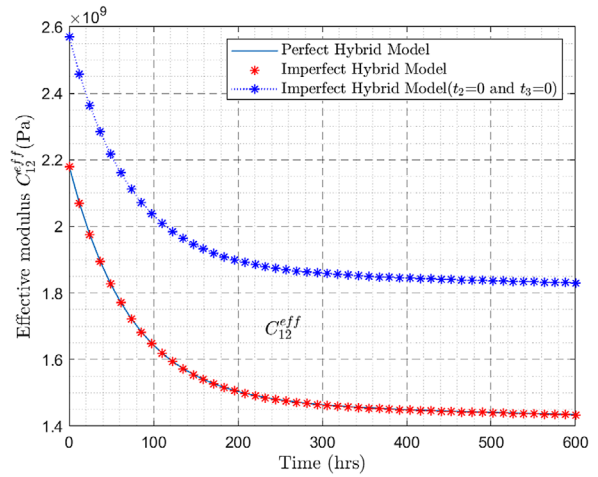


Figure 13d. Time dependent effective viscoelastic modulus C_{12}^{eff} for the three-layered viscoelastic composite with imperfect interfaces

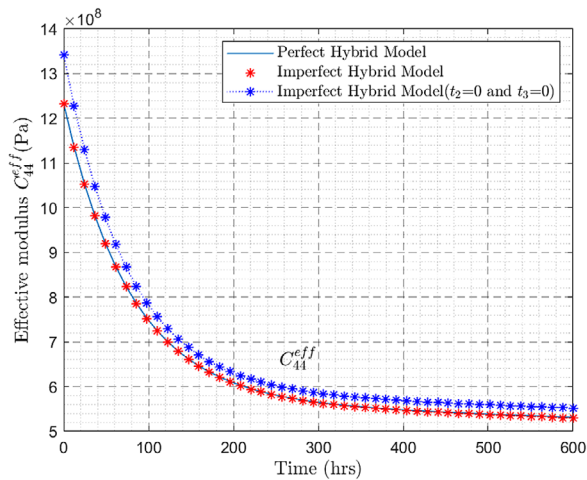


Figure 13e. Time dependent effective viscoelastic modulus C_{44}^{eff} for the three-layered viscoelastic composite with imperfect interfaces

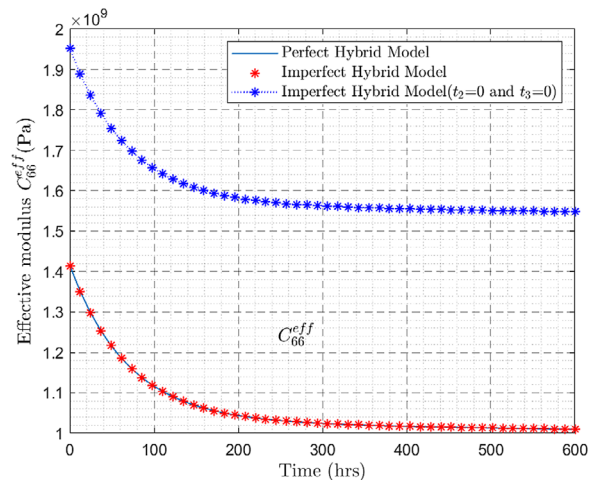


Figure 13f. Time dependent effective viscoelastic modulus C_{66}^{eff} for the three-layered viscoelastic composite with imperfect interfaces

interfaces. The sliding and debonding parameters of the viscoelastic imperfect interface are given as a function of the viscoelastic properties of the interface and its thickness. The viscoelastic behavior of the interface is described by the Maxwell’s model. Based on the Laplace transform, the effective properties are derived in the frequency domain and then inverted numerically based on the fixed Talbot algorithm to the time one. In the numerical results section, two kinds of composites are considered: a two-layered composite and a three-layered one. A comparison is made with the perfect hybrid model where the imperfect interfaces are

introduced as interlayers. It is demonstrated numerically that both models predict the same results in the frequency and time domain. Elliptic cycles are presented when harmonic uniaxial strain is applied on the two-layered composite for different frequency values. The elliptical cycles show the damping capacity of the considered composite. The effect of the thickness of the imperfect interfaces is also shown on the effective behavior in the case of the three-layered composite. The developed formalism is a contribution to designing multi-layered composites with damping characteristics for different engineering applications.

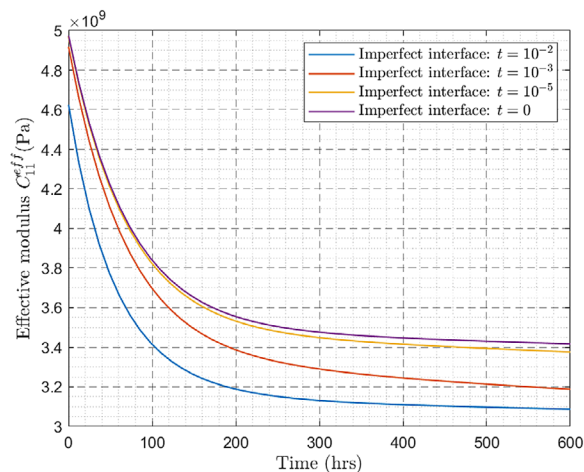


Figure 14. Time dependent effective viscoelastic modulus C_{II}^{eff} for the three-layered viscoelastic composite with different thicknesses of imperfect interfaces

REFERENCES

1. Hashin Z. Viscoelastic behavior of heterogeneous media. *Journal of Applied Mechanics*. 1965; 32: 630–636.
2. Hashin Z. Complex moduli of viscoelastic composites-I. General theory and application to particulate composites. *International Journal of Solids and Structures*. 1970a; 6: 539–552.
3. Hashin Z. Complex moduli of viscoelastic composites II: Fiber reinforced materials. *International Journal of Solids and Structures*. 1970b; 6: 797–807.
4. Christensen RM. Viscoelastic properties of heterogeneous media. *Journal of the Mechanics and Physics of Solids*. 1969; 17: 23–41.
5. Hashin Z. The elastic moduli of heterogeneous materials. *Journal of Applied Mechanics*. 1962; 29: 143–150.
6. Brinson LC, Lin WS. Comparison of micromechanics methods for effective properties of multiphase viscoelastic composites. *Composite Structures*. 1998; 41: 353–367.
7. Haberman MR, Berthelot Y, Jarzynski J, Cherkaoui M. Micromechanical modeling of viscoelastic composites in the low frequency approximation. *Journal of the Acoustical Society of America*. 2002; 112 (5): 1937–1943.
8. Haberman MR, Berthelot Y, Cherkaoui M. Transmission loss of viscoelastic materials containing oriented ellipsoidal coated micro inclusions. *Journal of the Acoustical Society of America*. 2005; 118 (5): 2984–2992.
9. Haberman MR, Berthelot Y, Cherkaoui M. Micromechanical modeling of particulate composites for damping of acoustic waves. *Journal of Engineering Materials and Technology*. 2006; 128: 320–329.
10. Cherkaoui M, Sabar H, Berveiller M. Micromechanical approach of the coated inclusion problem and applications to composite materials. *Journal of Engineering Materials and Technology*. 1994; 116: 274–278.
11. Koutsawa Y, Cherkaoui M, Daya EM. Multi-coating inhomogeneities problem for effective viscoelastic properties of particulate composite materials. Publication in *Journal of Engineering Materials and Technology*. 2009; 131(2): 021012 (11 pages).
12. Lipinski P, Barhdadi EH, Cherkaoui M. Micromechanical modeling of an arbitrary ellipsoidal multi-coated inclusion. *Philosophical Magazine*. 2006; 86 (10): 1305–1326.
13. Li R, Sun L Z. A micromechanics-based viscoelastic model for nanocomposites with imperfect interface. *International Journal of Damage Mechanics*. 2013; 22(7): 967-981.
14. Jiang B, Batra RC. Effective electroelastic properties of a piezocomposite with viscoelastic and dielectric relaxing matrix. *Journal of intelligent material systems and structures*. 2001; 12(12): 847–66.
15. Muliana A, Li KA. Time-dependent response of active composites with thermal, electrical, and mechanical coupling effect. *International journal of engineering science*. 2010; 48(11): 1481-1497.
16. Li JY, Dunn ML. Viscoelectroelastic behavior of heterogeneous piezoelectric solids. *Journal of Applied Physics*. 2001; 89: 2893–903.
17. Azrar L, Bakkali A, Aljinaidi AA. Frequency and time viscoelectroelastic effective properties modeling of heterogeneous and multi-coated piezoelectric composite materials. *Composite Structures*. 2014; 113: 281-297.
18. Bakkali A, Azrar L, Aljinaidi AA. Viscomagnetoelastic effective properties' modeling for multi-phase and multi-coated magnetoelastic composites. *Journal of Intelligent Material Systems and Structures*. 2016; 27(16): 2261-2286.
19. Lahellec, N, Suquet, P. Effective behavior of linear viscoelastic composites: a time-integration approach. *International Journal of Solids and Structures*. 2007; 44(2): 507-529.
20. Lahellec, N, Suquet, P. On the effective behavior of nonlinear inelastic composites: II: A second-order procedure. *Journal of the Mechanics and Physics of Solids*. 2007; 55(9): 1964-1992.
21. Ricaud JM, Renaud M. Effective properties of linear viscoelastic heterogeneous media: Internal variables formulation and extension to ageing behaviours. *International Journal of Solids and Structures*. 2009; 46 (7-8) : 1599-1606.
22. Masson R, Renald B, Olivier C. Incremental

- homogenization approach for ageing viscoelastic polycrystals. *Comptes Rendus Mécanique*. 2012; 340(4-5): 378-386.
23. Berbenni S, Florence D, Hafid S. A new internal variables homogenization scheme for linear viscoelastic materials based on an exact Eshelby interaction law. *Mechanics of Materials*. 2015; 81: 110-124.
 24. Sanahuja J. Effective behaviour of ageing linear viscoelastic composites: Homogenization approach. *International Journal of Solids and Structures*. 2013; 50(19): 2846-2856.
 25. El Kouri M, Bakkali A, Azrar L. Mathematical modeling of the overall time-dependent behavior of non-ageing viscoelastic reinforced composites. *Applied Mathematical Modelling*. 2016; 40(7-8): 4302-4322.
 26. El Kouri M, Bakkali A, Azrar L. Straightforward mathematical modeling of the time-dependent behavior of non-ageing viscoelastic composites with multi-coated inclusions. *Composite Structures*. 2018; 200: 689-700.
 27. Bakkali A, El Kouri M. Micromechanical modeling for the prediction of time-dependent effective properties and macroscopic coupled field response of polymer reinforced piezoelectric composites. *Applied Mathematical Modelling*. 2023; 120: 79-97.
 28. Barthélémy JF, Giraud A, Lavergne F, Sanahuja J. The Eshelby inclusion problem in ageing linear viscoelasticity. *International Journal of Solids and Structures*. 2016 ; 97: 530-542.
 29. Chen Y, Xin L, Liu Y, Guo Z, Dong L, Zhong Z. A viscoelastic model for particle-reinforced composites in finite deformations. *Applied Mathematical Modelling*. 2019; 72: 499–512.
 30. Chen Y, Yang P, Zhou Y, Guo Z, Dong , Busso EP. A micromechanics-based constitutive model for linear viscoelastic particle reinforced composites. *Mechanics of Materials*. 2020; 140: 103228.
 31. Chen Y, Zhao Z, Guo Z, Li Y. Micromechanical model of linear viscoelastic particle-reinforced composites with interphase. *Applied Mathematical Modelling*. 2021; 97: 308–321.
 32. Galadima YK, Oterkus S, Oterkus E, Amin I, El-Aassar A H, Shawky H. A nonlocal method to compute effective properties of viscoelastic composite materials based on peridynamic computational homogenization theory. *Composite Structures*. 2023; 319: 117147.
 33. Dinzart F. Viscoelastic behavior of composite materials with multi-coated ellipsoidal reinforcements and imperfect interfaces modeled by an equivalent inclusion. *Mechanics of Time-Dependent Materials*. 2023: 1-29.
 34. Molinari A. Averaging Models for Heterogeneous Viscoplastic and Elastic Viscoplastic Materials. *Journal of Engineering Materials and Technology*. 2002: 124(1), 62.
 35. Mercier S, Molinari A. Homogenization of elastic–viscoplastic heterogeneous materials: Self-consistent and Mori-Tanaka schemes. *International Journal of Plasticity*. 2009; 25(6): 1024–1048.
 36. Kowalczyk-Gajewska K, Petryk H. Sequential linearization method for viscous/elastic heterogeneous materials. *European Journal of Mechanics - A/Solids*. (2011); 30(5): 650–664.
 37. Kim JY. Effective elastic constants of anisotropic multilayers. *Mechanics Research Communications*. 2001; 28(1): 97–101.
 38. Bouchikhi A, Bakkali A, Ouardouz M. Prediction of the macroscopic behavior of multi-layered elastic composites. *MATEC Web of Conferences*. (2002); 360: 00011.
 39. Kim BC, Baltazar A, Kim JY. Effective Properties of Multi-layered Multi-functional Composites. *Advanced Composite Materials*. 2009; 18(2): 153–166.
 40. Kim JY. Micromechanical analysis of effective properties of magneto-electro-thermo-elastic multilayer composites. *International Journal of Engineering Science*. 2011; 49(9): 1001–1018.
 41. Stupkiewicz S, Petryk, H. Modelling of laminated microstructures in stress-induced martensitic transformations. *Journal of the Mechanics and Physics of Solids*. 2002; 50(11): 2303–2331.
 42. Berbenni S, Paliwal B, Cherkaoui M. A micromechanics-based model for shear-coupled grain boundary migration in bicrystals. *International Journal of Plasticity*. 2013; 44: 68-94.
 43. Tsekpuia E, Guery A, Gey N, Berbenni S. A microstructure-based three-scale homogenization model for predicting the elasto-viscoplastic behavior of duplex stainless steels. *International Journal of Plasticity*. 2023: 103575.
 44. Cruz-González OL, Rodríguez-Ramos R, Lebon F, Sabina FJ. Modeling of Imperfect Viscoelastic Interfaces in Composite Materials. *Coatings*. 2022; 12(5): 705.
 45. Talbot A. The accurate numerical inversion of Laplace transforms. *Journal of the Institute of Mathematics and Its Applications*. 1979; 23: 97–120.
 46. Hashin Z. The spherical inclusion with imperfect interface. *Journal of Applied Mechanics*. 1991a; 58 (6): 444–449.
 47. Hashin Z. Thermoelastic properties of particulate composites with imperfect interface. *Journal of the Mechanics and Physics of Solids*. 1991b; 39: 745–762.
 48. Kuo HY, Wu TJ, Pan E. Multilayer multiferroic composites with imperfect interfaces. *Smart Materials and Structures*. 2018; 27(7): 075032.